U.S. Department of Transportation
Federal Aviation Administration

FINAL PROJECT REPORT

Form Approved:
O.M.B. No. 2120-0559
9/30/2013

PART I - PROJECT IDENTIFICATION INFORMATION

1. Institution and Address	2. FAA Program	3. FAA Award Number
Massachusetts Institute of Technology	FAA Center of Excellence for Alternative Jet Fuels & Environme	13-C-AJFE-MIT
	4. Award Period From 3/29/2019 To 9/30/2024	5. Cumulative Award Amount 1,650,000

6. Project Title
Clean-Sheet Supersonic Aircraft Engine Design and Performance

PART II - SUMMARY OF COMPLETED PROJECT (For Public Use)

Engines for supersonic aircraft, compared with those for subsonic aircraft, present unique challenges in terms of fuel consumption, noise, and emissions impacts, because of their unique operating conditions. The propulsion systems currently proposed by the industry are derivative engines designed around the unmodified core (high-pressure compressor, combustor, and high-pressure turbine) of existing subsonic engines, with modifications to the low-pressure spool (fan and low-pressure turbine).

This project evaluates the design space of “clean-sheet” engines designed specifically for use on civil supersonic aircraft, and determines the resulting environmental performance of such engines. Unlike previous commercial supersonic engines adapted from military aircraft or planned propulsion systems derived from current commercial engines, a clean-sheet engine takes advantage of recent advances in propulsion system technology to substantially improve performance and reduce emissions and noise footprints.

This project quantifies these benefits for a range of engine designs relevant to currently proposed civil supersonic aircraft. In addition to characterizing conventional supersonic engine designs, the project also investigates more unconventional engine architectures, namely hybrid-electric systems. Finally, the project explores the use of advanced operational procedures to reduce noise during takeoff.

PART III - TECHNICAL INFORMATION (For Program Management Uses)

1. **ITEM** (Check appropriate blocks)	NONE	ATTACHED	PREVIOUSLY FURNISHED	TO BE FURNISHED SEPARATELY TO PROGRAM	
				Check (X)	Approx. Date
a. Abstracts of Theses		X			
b. Publication Citations		X			
c. Data on Scientific Collaborators		X			
d. Information on Inventions	X				
e. Technical Description of Project and Results		X			
f. Other (specify)					

2. Principal Investigator/Project Director Name (Typed)	3. Principal Investigator / Project Director Signature	4. Date
Raymond Speth	Raymond Speth	5/7/2025

FAA Form 9550-5 (03-03) Supersedes Previous Edition

Project 047 Clean-Sheet Supersonic Aircraft Engine Design and Performance

Supplement to FAA Form 9550-5

Thesis Abstracts

Title: Environmental Impacts of Future Aviation Propulsion Systems
Author: Prakash Prashanth
Date: October 27, 2022
URL: https://hdl.handle.net/1721.1/150129

Aviation is an integral part of modern society and economy. A fundamental challenge facing the aviation sector in the coming decades is to enable the 3.8% projected growth in air traffic per year and the associated benefits while simultaneously reducing aviation's impact on the environment in terms of air quality and climate. This thesis improves the scientific understanding of the atmospheric impacts attributable to aviation gas turbine emissions and the means of mitigating them with a focus on the propulsion system. Specifically, this thesis addresses aspects of 1) aerosol formation from aviation-attributable NO_x and SO_x, 2) the technical extent to which the air quality and climate impacts of aviation can be minimized, and 3) how propulsion system design for supersonic commercial aircraft in the future would impact the environment.

I first address how emissions of aerosol precursors species – NO_x and SO_x from aircraft gas turbine engines – results in aerosol formation. I quantify the contribution of the different pathways to the formation of secondary inorganic aerosol and their associated impact on radiative forcing and population exposure to pollutants at the surface. A key finding is that 47% of the aviation NO_x emissions-attributable aerosol RF is due to sulfate aerosol formed through the NO_x-sulfate pathway where, aviation-attributable oxidants derived from aviation NO_x emissions result in the oxidation of SO_x emissions to sulfate aerosol. Moreover, 88% of this sulfate related RF through the NO_x-sulfate pathway is due to the oxidation of nonaviation SO_x, highlighting the coupling between aviation and non-aviation emissions. Furthermore, I show that aviation emissions of NO_x are responsible for ~95% of aviation-attributable population exposure to particulate matter ($PM_{2.5}$) and ozone.

I then undertake the notional design of an aircraft system to assess whether it is technically feasible to have an aircraft system with net-zero climate impact and >95% reduction in air quality impacts relative to the present. The identified system relies on (1) an aviation fuel with low lifecycle greenhouse gas (GHG) emissions; (2) an aircraft design which accommodates post-combustion emissions control devices to enable a 96% reduction in emissions of NO_x; (3) operational strategies for contrail avoidance; and (4) atmospheric CO_2 removal with geological storage at small scale (1% of geological storage potential) to address GHG emissions which are otherwise prohibitively expensive to avoid. The proposed system reduces the combined climate and air quality impacts by 99% for a 16-22% increase in direct operating costs (excluding invested capital costs of aircraft and required infrastructure).

I then consider the environmental impacts that may arise from the addition of new capability in the form of commercial supersonic transport (SST) to the current system. Prior development of propulsion systems for SSTs have relied on derivative engines. I quantify the impact that constraints imposed by such a derivative engine design have on its performance relative to a clean-sheet design. Accounting for technology improvements, the clean-sheet design results in a 4% lower SFC than the derivative engine, with the SFC improvements being most sensitive to the ability to design low-NO_x combustors followed by turbomachinery efficiency. A fleet of 140 supersonic business jets using the derivative or clean-sheet engines result in ~13 mDU of column ozone depletion per billion available seat-kilometers in 2035.

This thesis (a) establishes the design trades and limitations of supersonic transport propulsion systems in terms of take-off noise reduction, (b) identifies the attributes, quantifies the potential, and assesses the impact of advanced take-off trajectories designed for noise reduction, and (c) formulates a reduced-order model to scale these results for supersonic transport of different size classes and cruise Mach numbers.

The propulsion system design trades established in this thesis show that clean- sheet engines do not enable supersonic transport to meet current subsonic transport noise limits when using conventional take-off trajectories. The impact of derivative engines on the cumulative noise levels is found to be small (1.4 EPNdB). In fact, regardless of whether a clean-sheet or derivative engine is selected, a Mach 1.4 business jet is shown to exceed the current cumulative noise limit by at least 15.5 EPNdB. Further noise reduction of the jet noise dominant engines is prevented by the fan size constraint imposed to limit wave drag during supersonic cruise.

Advanced trajectories are proposed to reduce take-off noise by capitalizing on excess engine thrust and improved aerodynamic efficiency at higher take-off speeds. These novel trajectories use (i) automatic continuous control of thrust and high-lift devices, (ii) increased take-off speed, and (iii) reduced cut-back altitude, compared to conventional trajectories currently used for subsonic transport. For the aircraft examined, although these trajectories reduce the 65 dB-A community noise contour area by 63.8%, they only reduce cumulative certification noise by 10.6 EPNdB, which is insufficient to meet current subsonic transport noise limits. Additionally, advanced trajectories with the lowest community noise do not yield the lowest certification noise, which warrants re-examination of supersonic transport noise standards. On the contrary, engine NO_x standards are representative for supersonic transport using advanced take-off trajectories and thus do not need to be modified, as the impact of these trajectories on the mass of NO_x emissions during climb-out is small (16.1%).

Last, a first-of-its-kind reduced-order model for supersonic transport take-off noise scaling shows that, as cruise Mach number increases, supersonic transport take-off noise levels increase while the thrust cut-back noise reduction potential decreases. This scaling rule enables equally stringent standard setting for noise certification of supersonic transport across a broad range of size classes and cruise Mach numbers.

Title: Modeling and Assessment of Efficiency in Arbitrary Air-Breathing Power Systems
Author: Wyatt Giroux
Date: May 16, 2024
URL: https://hdl.handle.net/1721.1/155392

The push for net-zero carbon emissions in the aviation sector by 2050 has resulted in an increasing amount of work being done to analyze the benefits of emergent technologies. Aircraft propulsion systems are a common subject of such research, and studies of some proposed architectures, such as hybrid-electric powertrains, have suggested potential fuel-burn and nitrogen oxide emissions reductions of up to 10% and 4.9%, respectively. When attempting to refine and compare these systems, efficiency is a commonly used metric. Efficiency models provide an understanding of where and how energy is being dissipated in a given system, making them invaluable design and evaluation tools. Until recently, the traditional thermal/propulsive efficiency breakdown has been used to model gas-turbine engines. However, this model has two major deficiencies. First, the lack of a per-component efficiency model restricts understanding of system energy dissipation to either thermodynamic or propulsive losses. Second, the traditional model is unable to capture systems utilizing additional energy sources (batteries, fuel cells, etc.) and their respective conversion pathways. While individual studies have created efficiency models for unconventional systems, these models are either specific to a given architecture or are only applicable to a specific class of engines. This makes comparison between specific terms in existing efficiency models impossible.

This thesis presents the Modular Efficiency Model (MEM), which is capable of constructing low-level efficiency models that accurately represent energy flow pathways and are algebraically consistent across arbitrary collections of propulsion system components. This is done by tracking the kinetic energy flow available for propulsion (expanded flow power) across each component in a system. MEM provides a more detailed breakdown of useful energy dissipation, relative influence of streams and components, and individual powertrain efficiencies that can be meaningfully compared to other systems. MEM is demonstrated in this work by comparing performance of unmixed, mixed-flow, and hybrid electric engine architectures. We identify high fan pressure ratio systems with low fan diameter as candidates for effective mixer use. For hybrid-electric systems, we find a 3.2% reduction in whole-mission fuel burn is possible at the cost of carrying only 50% of the original aircraft payload. Numerous detailed future studies utilizing MEM are recommended, using this thesis as a baseline example for the use of MEM in analyzing and comparing novel architectures.

Publication Citations

Voet, L., Prashanth, P., Speth, R., Sabnis, J., Tan, C., & Barrett, S. (2021, January 11–15 & 19–21). *The impact of design space constraints on the noise and emissions from derivative engines for civil supersonic aircraft*. AIAA Scitech 2021 Forum, virtual. https://doi.org/10.2514/6.2021-1272

Voet, L., Speth, R. L., Sabnis, J. S., Tan, C. S., & Barrett, S. R. (2022, June 14). *On the design of variable noise reduction systems for supersonic transport take-off certification noise reduction*. 28thAIAA/CEAS Aeroacoustics 2022 Conference, Southampton, United Kingdom. https://doi.org/10.2514/6.2022-3052

Voet, L., Speth, R., Sabnis, J., Tan, C., & Barrett, S. (2022). Sensitivities of aircraft acoustic metrics to engine design variables for multi-disciplinary optimization. *AIAA Journal*, *60*(8). https://doi.org/10.2514/1.J061411

Prashanth, P., Voet, L. J. A., Speth, R. L., Sabnis, J. S., Tan, C. S., & Barrett, S. R. H. (2023). Impact of Design Constraints on Noise and Emissions of Derivative Supersonic Engines. *Journal of Propulsion and Power*, *39*(3), 1–10. https://doi.org/10.2514/1.B38918

Voet, L. J. A., Prashanth, P., Speth, R. L., Sabnis, J. S., Tan, C. S., & Barrett, S. R. H. (2024). Automatic Continuous Thrust Control for Supersonic Transport Takeoff Noise Reduction. *Journal of Aircraft*, *61*(1), 291–306. https://doi.org/10.2514/1.C037394

Voet, L. J. A., Prashanth, P., Speth, R. L., Sabnis, J. S., Tan, C. S., & Barrett, S. R. H. (2024). Reduced-Order Model for Supersonic Transport Takeoff Noise Scaling with Cruise Mach Number. *Journal of Aircraft*, *61*(4), 1155–1168. https://doi.org/10.2514/1.C037633

Data on Scientific Collaborators

- Steven Barrett, Professor (P.I.)

- Raymond Speth, Principal Research Scientist (Co-P.I.)
- Choon Tan, Senior Research Engineer (Co-P.I.)
- Jayant Sabnis, Senior Lecturer (Co-I.)
- Prakash Prashanth, Graduate Student
- Laurens Voet, Graduate Student
- Wyatt Giroux, Graduate Student

Project 047 Clean-Sheet Supersonic Aircraft Engine Design and Performance

Massachusetts Institute of Technology

Project Lead Investigator

Steven R. H. Barrett
Professor of Aeronautics and Astronautics
Department of Aeronautics and Astronautics
Massachusetts Institute of Technology
77 Massachusetts Avenue
Cambridge, MA 02139
617-452-2550
sbarrett@mit.edu

University Participants

Massachusetts Institute of Technology (MIT)

- P.I.: Prof. Steven R. H. Barrett
- FAA Award Number: 13-C-AJFE-MIT, Amendment Nos. 052, 059, 074, 076, 090, 106, 110, and 115 (NCE to September 30, 2024)
- Period of Performance: March 29, 2019, to September 30, 2024
- Tasks:
  1. Identify mission profiles and operating requirements for propulsion systems
  2. Develop an engine cycle model for a supersonic aircraft propulsion system
  3. Assess environmental footprint of an engine for a supersonic transport aircraft
  4. Evaluate the impact of improved technology on relative performance benefits of clean-sheet and derivative engines
  5. Evaluate the effects of fan diameter and unconventional architectures on the environmental impacts of clean-sheet engines
  6. Assess the effect of variable noise reduction systems on landing and take-off (LTO) emissions for engines for supersonic transport aircraft
  7. Evaluate the impact of advanced take-off trajectories for supersonic transport (SST) using variable noise reduction systems on community noise

Project Funding Level

The ASCENT Project 047 received $1,650,000 in Federal Aviation Administration (FAA) funding and $1,650,000 in matching funds. Sources of matching funds are approximately $340,000 from MIT, plus third-party in-kind contributions of $177,000 from Byogy Renewables, Inc.; $982,000 from NuFuels, LLC; and $151,000 from Savion Aerospace Corporation.

Investigation Team

Prof. Steven Barrett, (P.I.), Tasks 1-7
Dr. Raymond Speth, (co-P.I.), Tasks 1-7
Dr. Choon Tan (co-P.I.), Tasks 1-7
Dr. Jayant Sabnis, (co-investigator), Tasks 1-7
Dr. Prakash Prashanth, (graduate student), Tasks 1, 2, 3, 4, and 5
Dr. Laurens Voet, (graduate student), Tasks 1, 3, 6, and 7
Mr. Wyatt Giroux, (graduate student), Task 5

Project Overview

Engines for supersonic aircraft, compared with those for subsonic aircraft, present unique challenges in terms of fuel consumption, noise, and emissions impacts, because of their unique operating conditions. The propulsion systems currently proposed by the industry are derivative engines (Figure 1) designed around the unmodified core (high-pressure compressor, combustor, and high-pressure turbine) of existing subsonic engines, with modifications to the low-pressure spool (fan and low-pressure turbine).

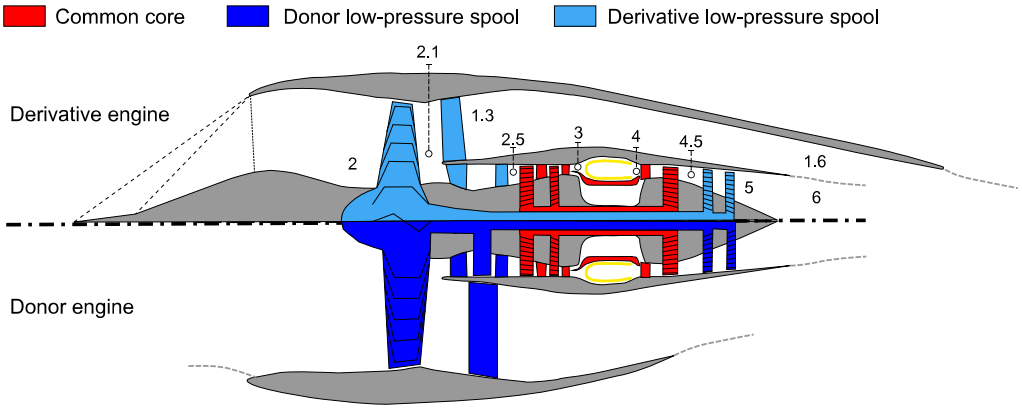

Figure 1. Engine architecture schematic. The lower half shows the subsonic donor engine. The high-pressure spool (red) core is used in the derivative engine (top half) along with modifications to the inlet, fan, and nozzle, as shown in the top half.

This project is aimed at evaluating the design space of "clean-sheet" engines designed specifically for use on civil supersonic aircraft, and to determine the resulting environmental performance of such engines. Unlike previous commercial supersonic engines, which were adapted from military aircraft, or planned propulsion systems derived from current commercial engines, a clean-sheet engine takes advantage of recent advances in propulsion system technology to substantially improve performance and reduce emissions and noise footprints. This project will quantify these benefits for a range of engine designs relevant to currently proposed civil supersonic aircraft. Conventional clean-sheet engines have been examined by the ASCENT Project 047 team. To further characterize the clean-sheet design space, more unconventional engine architectures, namely hybrid-electric systems, are investigated. Specifically, we aim to assess the relative performance of hybrid-electric clean-sheet and conventional clean-sheet engines.

Task 1 - Identify Mission Profiles and Operating Requirements for Propulsion Systems

Massachusetts Institute of Technology

Objectives

The objectives of this task are to (1) identify representative mission profiles of commercial SST aircraft (i.e., characterize stages of the mission by defining parameters such as climb rates and accelerations) and (2) use these mission profiles and representative aircraft parameters (e.g., wing area, drag and lift polars) of civil supersonic aircraft operating in different Mach regimes to derive propulsion system requirements for supersonic aircraft.

Research Approach

Design Space Survey

In Figure 2, the ASCENT Project 047 team presents a set of SST aircraft concepts and existing designs with their respective range and cruise Mach (M) number.

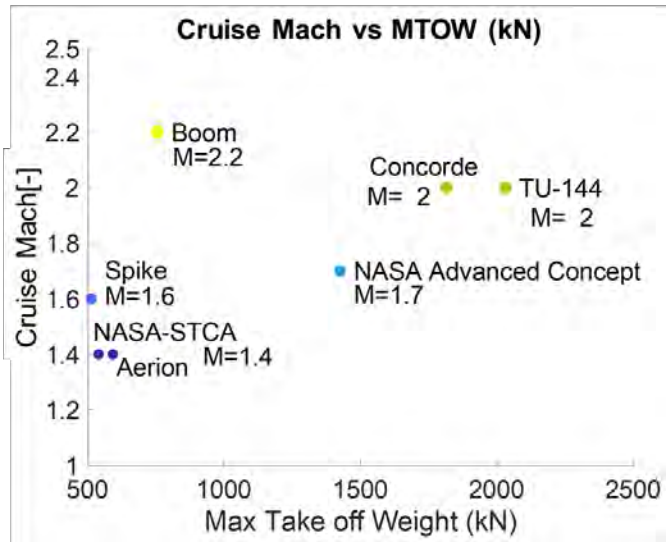

Figure 2. Range versus maximum take-off weight for civil SST aircraft concepts and existing designs.

Figure 2 shows the variability of different concepts and designs for SST. The only existing designs are the Anglo-French Concorde and the Russian Tupolev TU-144 in the Mach 2 regime. However, upcoming companies looking to bring SST back to the market are developing aircraft in different Mach regimes, including low-supersonic (M~1.4), mid-supersonic (M~1.6), and high-supersonic (M~2), and in different weight classes: small business jets and larger airliners.

Mission Profiles

The only existing SST aircraft were the Concorde and Tupolev TU-144. Morisset (1974) compared their performance and shows their mission profiles. A typical mission profile of Concorde is shown in Figure 3. This mission profile is chosen as a case to test the tool to derive propulsion system requirements for an SST aircraft. The mission profile is modeled in SUAVE (Lukaczyk et al., 2015). A comparison of the mission profiles is shown in Figure Figure 3. The descent profile in SUAVE is modeled as a single mission stage because it is assumed that the propulsion requirements during descent will not be critical.

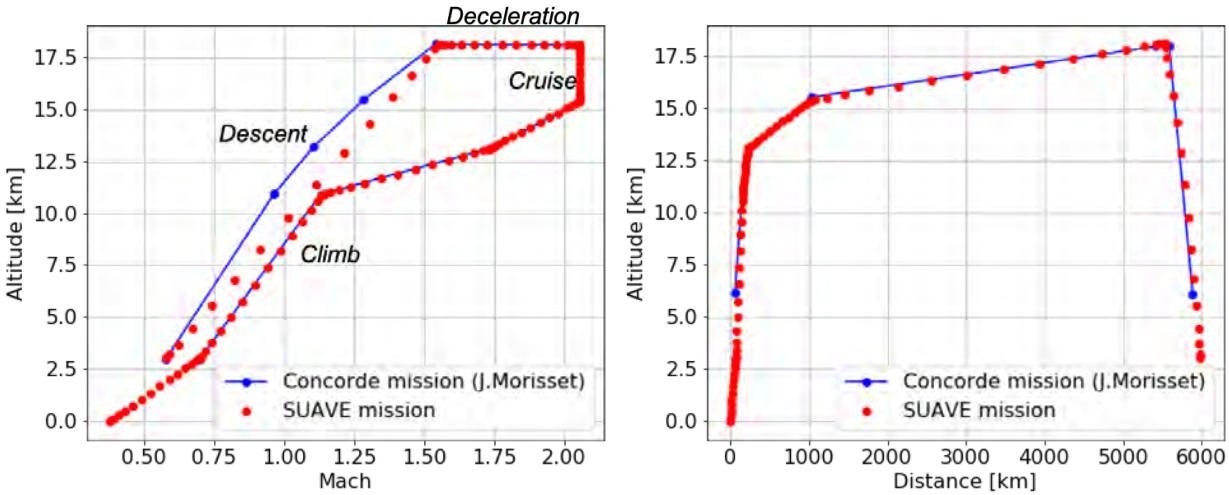

Figure 3. Typical mission profile of Concorde.

Propulsion System Requirements

The SUAVE tool is used to estimate propulsion system requirements for the Concorde aircraft based on the Concorde flight reports (Morisset, 1974). The standard aircraft parameters and aerodynamic coefficients of the Concorde aircraft from the SUAVE tool are used. The propulsion system requirements (i.e., thrust) of the Concorde mission are given in Figure 4 (top). The variation in the drag coefficient of the aircraft during the mission is given in Figure 4 (bottom). The discontinuities in the thrust profile come from jumps in climb rates and in acceleration rates. In Figure 4, the drag coefficient can be seen to sharply increase when crossing the sound barrier. From the thrust profile, the most critical points in the mission can be identified. The engine will need to be able to generate the specified thrust at these points. Therefore, the thrust at these critical points will be a direct input in Task 2 when developing the engine cycle model.

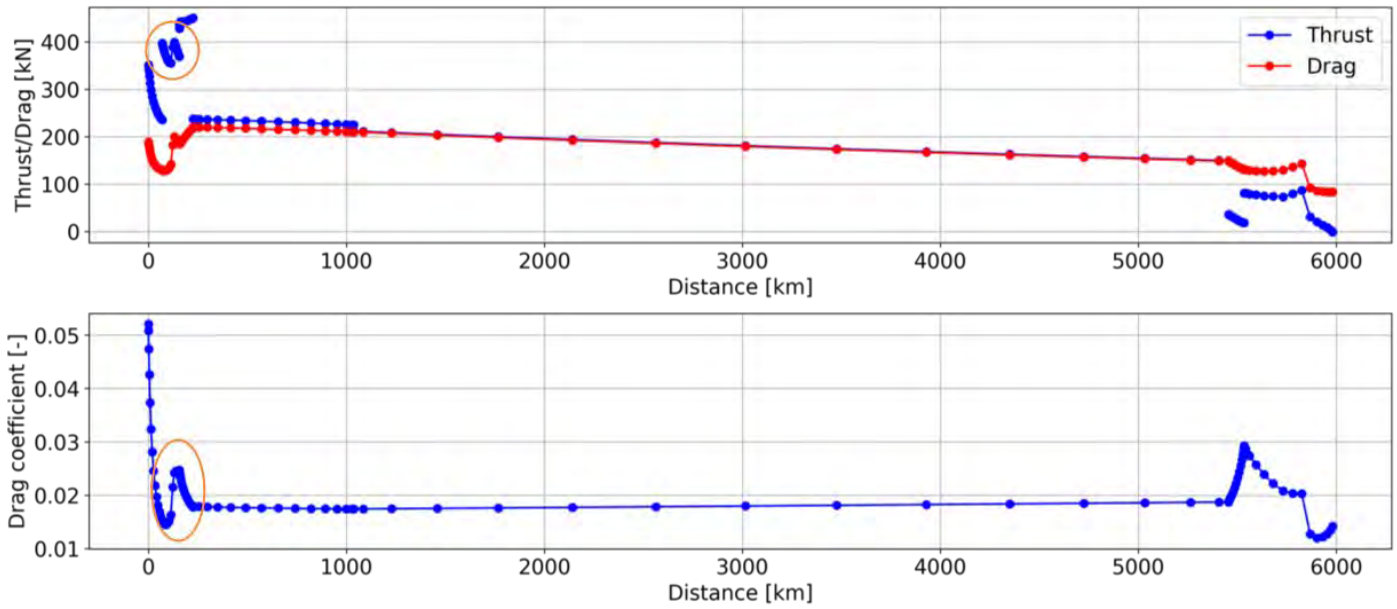

Figure 4. Propulsion system requirements (i.e., thrust and drag) and drag coefficient throughout the mission given in Figure 3. The circled areas indicate the transonic acceleration.

NASA 55-tonne STCA

The National Aeronautics and Space Administration (NASA) has designed a 55-tonne Supersonic Transport Concept Aircraft (STCA) with a cruise Mach number of 1.4 (Berton & Geiselhart, 2019). The aircraft configuration of the STCA is used to derive propulsion system requirements for a small business jet in the low-supersonic Mach regime. The four critical sizing points of the NASA STCA, as illustrated in Table 1, are used in a multiple-design-point (MDP) model in the engine design process.

Table 1. Propulsion system requirements (per engine) for STCA. The top-of-climb conditions are chosen as the aerodynamic design point for any component that is purpose designed for the application.

	Sea Level Static (SLS)	Take-off (TO)	Top-of-climb (TOC)	End-of-cruise (EOC)
Altitude [kft]	0	0	41	51
Mach [-]	0	0.25	1.4	1.4
Thrust [lbf]	16,617	14,140	5,500	3,300

Mission requirements for other aircraft designs will be obtained through collaborations with ASCENT Project 010.

M2.2 Medium SST – 55 passengers, Mach 2.2 Airliner
The mission requirements of a 55-passenger, 4-engine, Mach 2.2 SST – designed by the Georgia Institute of Technology – have been obtained through collaboration with the ASCENT 010 Project.

Milestone(s)

- Conducted a review of the SST concepts and existing designs.
- Identified the appropriate tools to derive propulsion system requirements for an SST aircraft flying a specific mission.

Major Accomplishments

- Conducted a survey of SST concepts and existing designs. Upcoming players in the SST market are developing aircraft in different Mach regimes (i.e., low-, mid-, and high-supersonic regimes) and weight classes (i.e., business jet and airliner).
- Selected SUAVE to derive propulsion system requirements for a supersonic aircraft flying a specific mission profile. For the specific case of a small business jet in the low-supersonic Mach regime, the NASA 55-tonne STCA aircraft (Berton & Geiselhart, 2019).

Publications

None.

Outreach Efforts

- Contacted Boom Supersonic to discuss representative mission profiles and aircraft parameters.
- Prof. Steven Barrett gave a presentation titled "Clean-sheet supersonic engine design and performance" at the ASCENT meeting in Atlanta, GA, on April 19, 2019.
- Dr. Jayant Sabnis gave a presentation titled "Clean-sheet supersonic engine design and performance" at the ASCENT meeting in Alexandria, VA, on October 22, 2019.

Awards

None.

Student Involvement

This task was conducted primarily by Mr. Prakash Prashanth and Mr. Laurens Voet, graduate research assistants working under the supervision of Dr. Jayant Sabnis, Dr. Raymond Speth, and Dr. Choon Tan.

References

Berton, J., & Geiselhart, K. (2019). *NASA 55 tonne Supersonic Transport Concept Aeroplane (STCA) release package*. NASA Glenn Research Center & NASA Langley Research Center.

Lukaczyk, T., Wendorff, A. D., Botero, E., MacDonald, T., Momose, T., Variyar, A., Vegh, M. J., Colonno, M., Economon, T. D., Alonso, J. J., Orra, T. H., and da Silva, C. I. (2015, June 22-26). *SUAVE: An open-source environment for multi-fidelity conceptual vehicle design* [Conference presentation]. 16th AIAA/ISSMO Multidisciplinary Analysis and Optimization Conference, Dallas, Texas. https://doi.org/10.2514/6.2015-3087

Morisset, J. (1974). *Tupolev 144 and Concorde – The official performances are compared for the first time* (NASA-TT-F-15446). NASA. https://ia800507.us.archive.org/11/items/nasa_techdoc_19740011548/19740011548.pdf

Task 2 - Develop an Engine Cycle Model for a Supersonic Aircraft Propulsion System

Massachusetts Institute of Technology

Objective

The objective of this task was to develop an engine cycle deck to analyze clean-sheet and derivative propulsion systems for commercial supersonic aircraft.

Research Approach

The Numerical Propulsion System Simulation (NPSS) tool is chosen to develop the engine cycle decks for clean-sheet and derivative engines, because it is an industry standard tool that facilitates future collaboration with other users of the tool.

Baseline Engine

To develop the derivative engine, a baseline engine is first chosen and modeled. The CFM56-5B engine was chosen for this task because it is the donor engine for the proposed GE Affinity engine. The baseline engine was modeled using published data from Jane's Aero Engines (Gunston, 1996) and data published in the Engine Emissions Databank (EEDB) by the European Union Aviation Safety Agency (EASA) (EASA, 2019). The data published by EASA consist of fuel flow and emission indices of several species at take-off, climb, idle, and approach conditions of various thrust variants of the CFM56-5B engine. The EEDB data can be processed based on the serial number of the tested engines to relate multiple entries in the databank to a common engine, as shown in Figure 5.

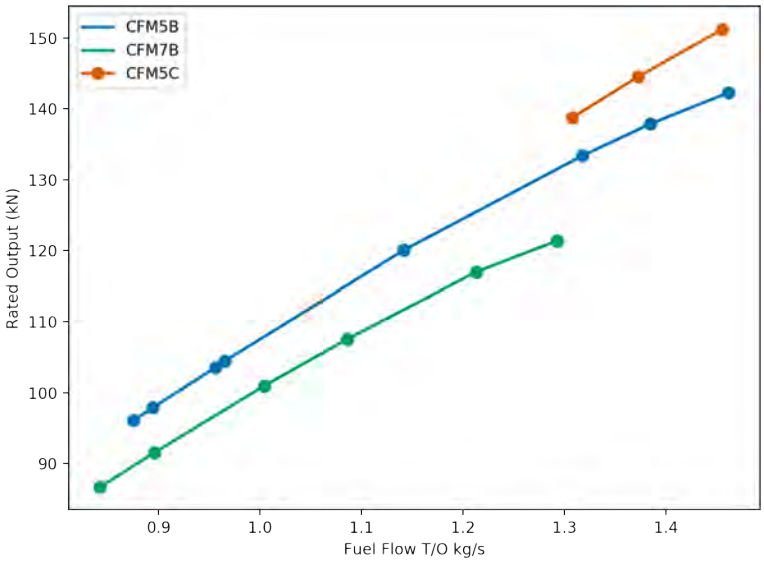

Figure 5. Variants of the CFM56 engine; the CFM56-5B Tech Insertion engine is chosen for the baseline engine.

The engine model (see schematic below) consists of an inlet, fan, low-pressure compressor (LPC), high-pressure compressor (HPC), combustor, high-pressure turbine (HPT), low-pressure turbine (LPT), and nozzles for the bypass and core ducts.

Component parameters such as efficiencies, pressure ratios, and bleed flows for the engine model were varied at a chosen design point. The point chosen for this was the sea-level static thrust of the highest thrust variant of the engine. Subsequent off-design runs were carried out to evaluate whether the model matched the published data on fuel flow at particular thrust levels.

Furthermore, the CFM56-5B and CFM56-7B engines share the same physical core. This information is used to validate the model representing the core specifically by using the core model calibrated to the CFM56-5B data to represent the CFM56-7B engine, by fixing the core components and varying only the low-spool components.

Derivative Engine Model

The thrust requirements of the derivative engine are given in Table 1. As shown in the engine architecture diagram in Figure 1, the derivative engine for supersonic application uses the high-pressure core of the donor subsonic engine. The low-pressure spool consists of a two-stage fan and LPT. An external compression supersonic inlet with two oblique shocks is mounted upstream of the fan, with a pressure recovery modeled using standard oblique shock equations. A fully mixed, variable area nozzle is added downstream of the LPT. The engine is designed such that the nozzle is at the cusp of choke at

take-off conditions to avoid shock-cell noise. Polytropic efficiencies of the turbomachinery components are set to values representative of the CFM56-5B3 technology level. The map scalars of the turbomachinery components in the engine cycle model, the flow areas, and the cooling bleed flow fractions of the CFM56 donor engine core are applied as fixed constants to the derivative engine model.

Clean-Sheet Engine Model
The clean-sheet engine is also designed to meet the propulsion system requirements outlined in Table 1. The engine architecture for the clean-sheet design is the same as the derivative design. However, all the components for the clean-sheet engine, along with the high-pressure core, are purpose-designed. To have a fair comparison between the derivative and clean-sheet engine, the polytropic efficiencies of the turbomachinery are set to the CFM56 values to model the same technology level and turbine cooling flow requirements are met using semi-empirical methods.

Engine Performance Sensitivities
An optimizer coupled with the NPSS models is used to optimize the cycle subject to any constraints (temperature limits and fan diameter limits) for various thrust requirements.

Environmental Footprint Calculations
A first-principles approach is used to evaluate design space constraints imposed by the donor core on the environmental footprint of the derivative engine. The engine cycle deck described above is used to calculate the engine performance in terms of specific fuel consumption (SFC), emissions index and noise of both the derivative and clean-sheet engine. Engine gaseous nitrogen oxides (NO_x) emissions are quantified using the P_3-T_3 method (DuBois & Paynter, 2006). The emission index of NO_x is assumed to be proportional to $P_{t3}^{0.4}$ and a polynomial fit in T_{t3}, constructed based on engine emission data from the International Civil Aviation Organization (ICAO) emission databank, leading to the correlation

$$\frac{\mathrm{EI(NO_x)}}{P_{t3}^{0.4}} = 6.26 \cdot 10^{-8} T_{t3}^3 - 0.00117 T_{t3}^2 + 0.0074 T_{t3} - 15.04 \qquad \text{(Eq. 1)}$$

The aircraft certification cumulative noise levels are computed based on standard methods as summarized in Task 3 (see Table 2).

Milestones

- Developed multiple engine models in NPSS. The donor engine for the supersonic derivative core is chosen to be the CFM56-5B engine.
- Used the derivative engine model to evaluate the impact of design space constraints on the performance of the engine relative to the clean-sheet model.
- Compared the performance of the clean-sheet engine and derivative engines for different thrust requirements.

Major Accomplishments

CFM56-5B3 Model Calibration
Publicly published data were used to build a CFM56-5B3 model in NPSS and calibrate the model at sea-level static conditions as shown in Figure 6.

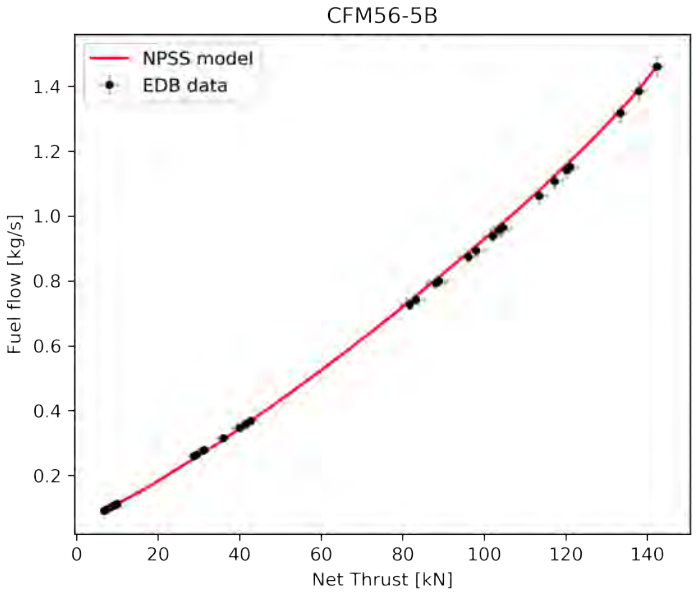

Figure 6. Off-design comparison of the NPSS model and ICAO data from the EEDB for the CFM56-5B engine.

The model is compared with the data available in the EEDB maintained by EASA on behalf of ICAO. The average root mean square (RMS) error for all the landing and take-off (LTO) data points is approximately 2%, suggesting a successful calibration.

The same core is used in a CFM56-7B engine and compared with EEDB data as shown in Figure 7. The average RMS error was approximately 3% in this case (Figure 7).

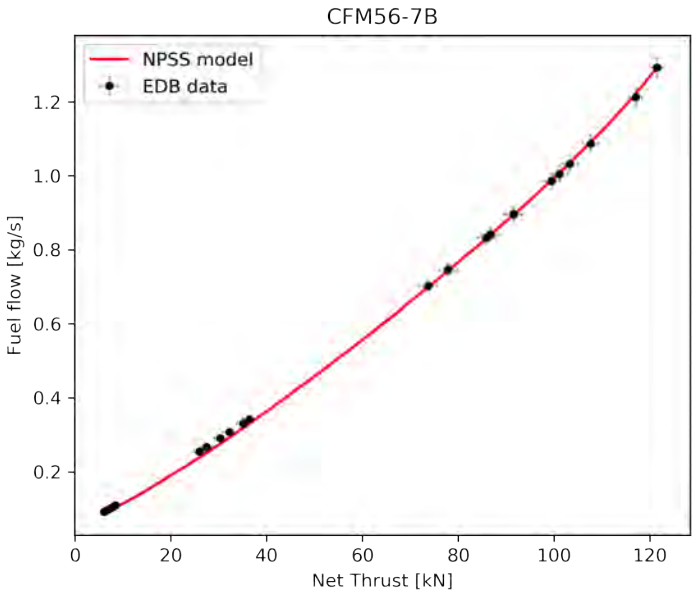

Figure 7. Off-design comparison of the NPSS model and ICAO data from the EEDB for the CFM56-7B engine using the common core.

Derivative Engine Design Space Constraints

Since the core of the derivative engine is sized by the donor-engine (CFM56) cycle, the pressure ratio of the HPC of the derivative engine is not an independent design variable (in contrast to a clean-sheet engine where the HPC pressure ratio is a design variable that can be optimized). The design space of the derivative engine is illustrated in Figure 8. The core of the derivative engine also has cooling flows for the high-pressure turbine sized by the donor engine cycle. Therefore, there are regions of the design space where insufficient cooling flow can result in turbine blade metal temperatures exceeding the set limits. Therefore, the constraints from the donor core limit the feasible design space that can be used for the derivative engine.

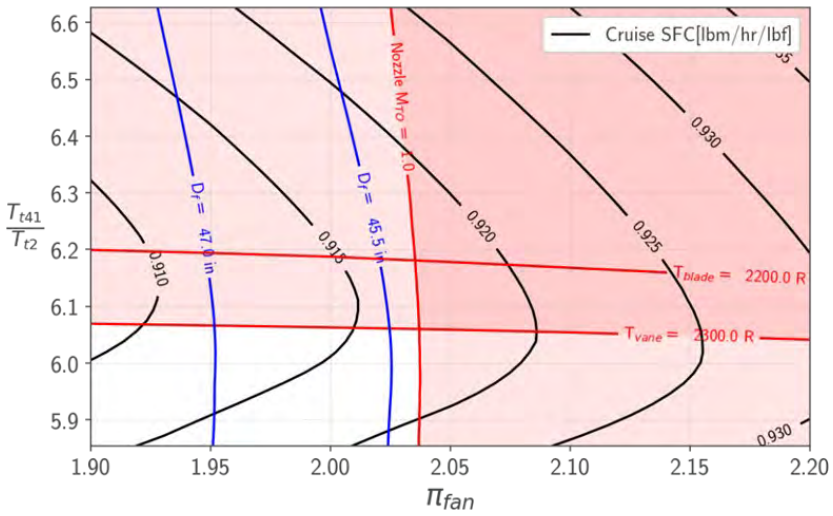

Figure 8. Design space of the derivative engine: turbine inlet temperature over compressor inlet temperature ratio, T_{t41}/T_{t2}, vs. fan pressure ratio, π_{fan}, at the engine aerodynamic design point. The performance contours show the cruise SFC. The resulting fan diameter, D_f, for different designs in the design space is indicated.

Engine Performance Sensitivities

The required thrust of the aircraft impacts the performance of the clean-sheet and derivative engines. At each thrust level, the clean-sheet and derivative engine are optimized to provide minimum SFC. Figure 9 shows the impact that the thrust required has on the fuel consumption and emissions of NO_x. The fan size for both engines is constrained to be 45.5 in. (consistent with the STCA airframe requirement).

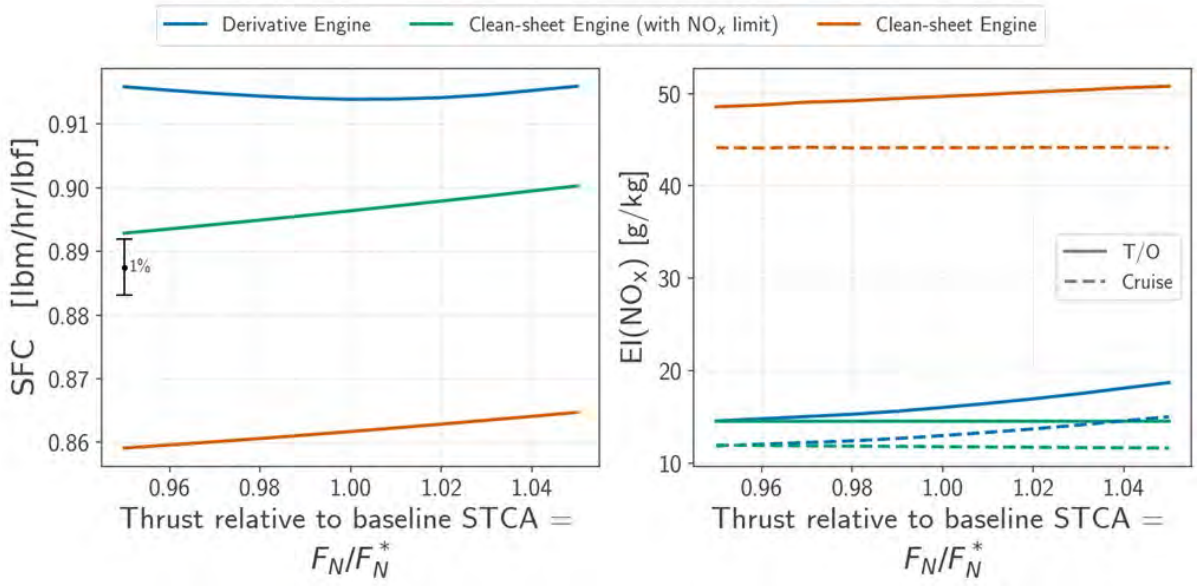

Figure 10. Sensitivities of engine performance parameters (specific fuel consumption at cruise, $\boldsymbol{SFC}$, and NO_x emission index, $\boldsymbol{EINO_x}$, at both design and sea-level static take-off conditions) for a range of thrust requirements. The thrust required is shown as a fraction of the STCA design thrust.

As seen in Figure 11, the clean-sheet engine designed for minimum SFC results in a 5.5 – 6.5% reduction in SFC relative to the derivative. However, assuming the same combustor technology is applied in the clean-sheet engine as the derivative, the emissions of NO_x from the clean-sheet engine that is optimized for minimum SFC is approximately three times greater than the derivative engine. An alternate clean-sheet engine sizing strategy is to impose a NO_x emissions constraint. This results in a 2-3% reduction in SFC relative to the derivative engine. This highlights the need to switch to advanced combustor designs that minimize NO_x emissions if the potential SFC benefits of a clean-sheet engine design are to be realized.

Publications

Voet, L., Prashanth, P., Speth, R., Sabnis, J., Tan, C., & Barrett, S. (2021, January 11–15 & 19–21). *The impact of design space constraints on the noise and emissions from derivative engines for civil supersonic aircraft* [Conference presentation]. AIAA Scitech 2021 Forum, virtual.

Prashanth, P., Voet, L. J. A., Speth, R. L., Sabnis, J. S., Tan, C. S., & Barrett, S. R. H. (2023). Impact of Design Constraints on Noise and Emissions of Derivative Supersonic Engines. *Journal of Propulsion and Power*, *39*(3), 1–10. https://doi.org/10.2514/1.B38918

Outreach Efforts

- Dr. Jayant Sabnis gave a presentation titled “Noise and emission characteristics of commercial supersonic aircraft propulsion systems” at the Aviation Noise and Emissions Symposium on March 5, 2019.
- Mr. Prashanth Prakash and Mr. Laurens Voet gave a presentation titled “Clean-sheet supersonic engine design and performance” at the at the virtual ASCENT meeting on September 30, 2020.
- Mr. Prashanth Prakash and Mr. Laurens Voet gave a presentation titled “Clean-sheet supersonic engine design and performance” at the virtual ASCENT meeting on April 27, 2021.
- Mr. Prashanth Prakash gave a presentation titled “Civil Supersonic Transport Emissions” at the Aviation Emissions Characterization Roadmap 2021 Annual Meeting on May 26, 2021.

Awards

None.

Student Involvement

This task was conducted primarily by Prashanth Prakash, a graduate research assistant working under the supervision of Dr. Jayant Sabnis, Dr. Raymond Speth, and Dr. Choon Tan.

References

DuBois, D., & Paynter, G. C. (2006). Fuel Flow Method 2 for estimating aircraft emissions (SAE Technical Paper 2006-01-1987). SAE International.

EASA (2019). ICAO Aircraft Engine Emissions Databank, version 26A. European Union Aviation Safety Agency (EASA). https://www.easa.europa.eu/easa-and-you/environment/icao-aircraft-engine-emissions-databank

Gunston, B. (1996). *Jane's aero-engines*. Jane's Information Group.

Task 3 - Assess Environmental Footprint of an Engine for a Supersonic Transport Aircraft

Massachusetts Institute of Technology

Objective

The objective of this task is to develop models to assess the environmental footprint of an SST aircraft. Models for both the noise footprint and the emissions footprint will be developed.

Research Approach

The flow chart in Figure 10 illustrates the approach to model the environmental footprint of engines for SST.

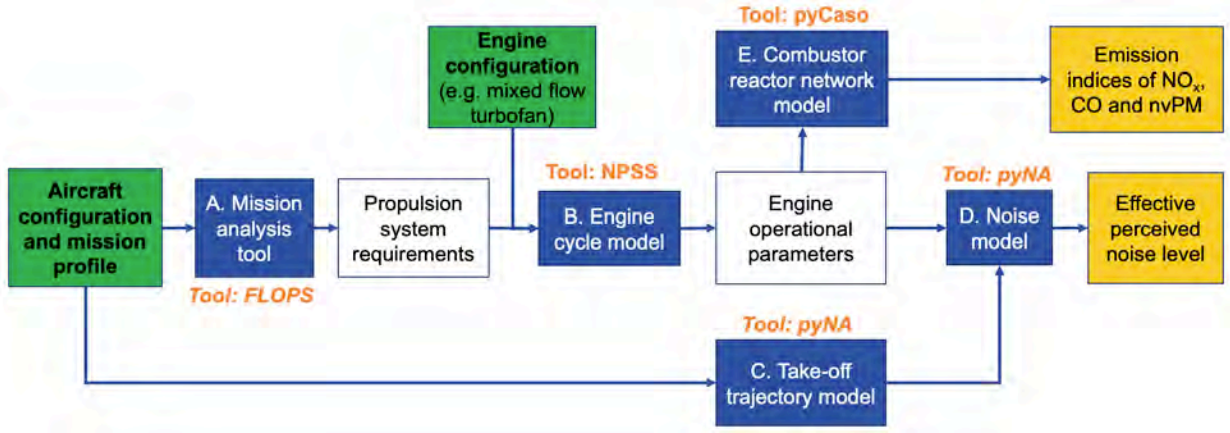

Figure 12. Overview of the framework to model environmental footprint of engines for SST. The mission analysis is performed using the NASA Flight Optimization System (FLOPS) software, the engine cycle model is made in the NPSS tool, the combustor reactor network model (pyCaso) and the aircraft noise and take-off trajectory model (pyNA) are used to calculate emission indices and effective perceived noise levels of the engines.

Emissions Modeling

A chemical reactor network combustor model (pyCaso) was developed to assess the emissions of the engines for SST. The combustor model represents CFM56-TechInsertion rich-quench-lean (RQL) combustor technology. The combustor model is illustrated in Figure 11. A series of perfectly stirred reactors in parallel, representing the primary zone of the combustor, are coupled to a secondary zone plug flow reactor. Similar to the engine model, the emission characteristics of the combustor model are validated against publicly available data from the EEDB.

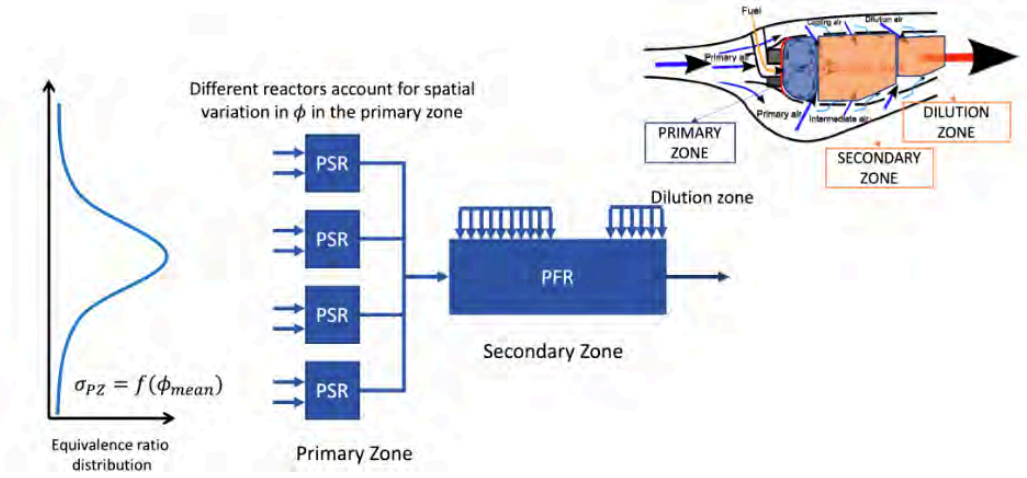

Figure 13. Chemical reactor network combustor model: a series of perfectly stirred reactors (PSR) in parallel, representing the primary zone, combined in parallel with a secondary zone plug flow reactor (PFR). The series of perfectly PRF represents a gaussian distribution, with standard deviation, $\boldsymbol{\sigma_{PZ}}$ being a function of the mean equivalence ratio, $\boldsymbol{\phi_{mean}}$.

Noise Footprint Modeling

A Python Noise Assessment (*pyNA*) model was developed to estimate the engine certification noise levels and assess their sensitivities with respect to engine operating variables. The model is developed in Python within the OpenMDAO framework (Gray et al., 2019); the individual noise modules have been implemented in Julia to be able use its automatic differentiation (AD) libraries for the Jacobian computation. The different noise modules in *pyNA,* as shown in Figure 12, are developed based on the methods from literature listed in Table 2, based on the NASA Technical Memorandum TM-83199 (Zorumski, 1982). The extended design structure matrix (Lambe et al, 2012) of the aircraft noise estimation model is shown in Figure 12.

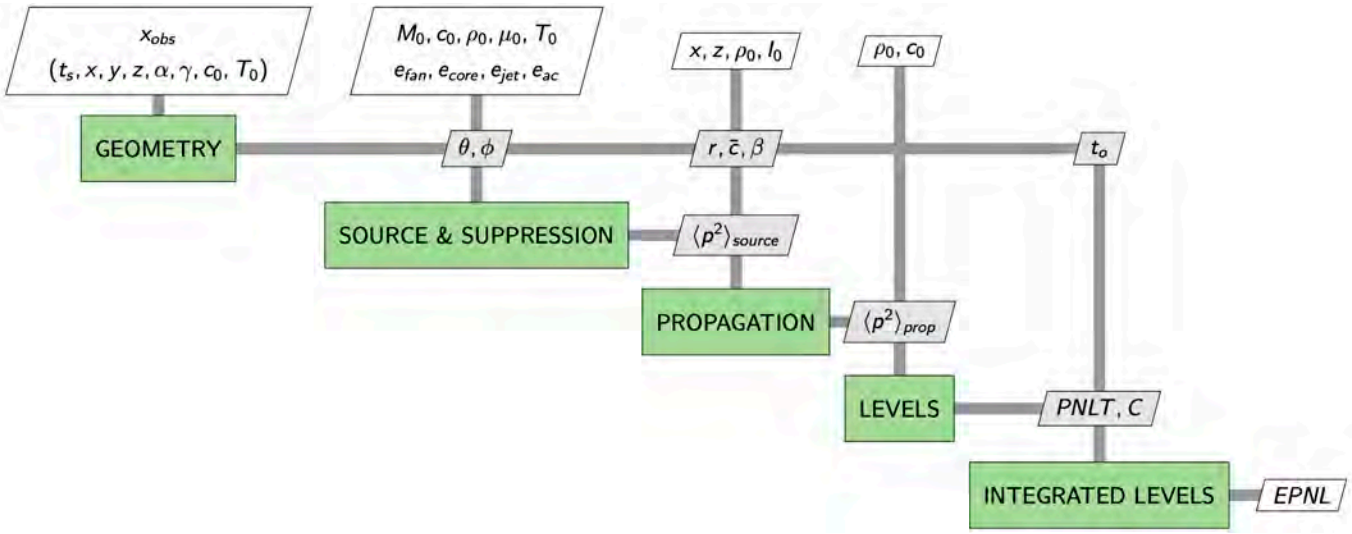

Figure 14. Flow chart of the pyNA model with the different modules required to estimate the effective perceived noise level (EPNL) from engine cycle and fan parameters.

Table 2. Methods for the noise source, propagation, and levels modules.

Module	Method from literature
Noise source modules • Jet mixing noise • Jet shock-cell noise • Combustor noise • Fan broadband and tones (inlet and discharge) • Airframe noise	Single-stream, shock-free jet mixing noise (SAE International, 2021) Circular jet shock cell noise (SAE International, 2021) Emmerling method FAA-RD-74-125 (Emmerling et al., 1976) Heidmann method NASA TM X-71763 (Heidmann, 1979) • with GE Aircraft Engines revision NASA CR-195480 for broadband (Kontos et al., 1996a) • with AlliedSignal revision for fan tones (Hough & Weir, 1996) • with fan treatment NASA CR-202309 (Kontos et al., 1996b) Fink method FAA RD-77-29 (Fink, 1977) • with HSR calibration *NASA CR-2004-213014 (*Golub et al., 2004)
Noise propagation modules • Spherical spreading/characteristic impedance • Atmospheric absorption • Ground reflection and attenuation • Lateral attenuation • Wing shielding module	R^2 law and characteristic impedance ratio Exponential decay using atmospheric absorption coefficient (Montegani, 1979) Chien-Soroka method (Chien & Soroka, 1975) SAE AIR 5662 method (SAE International, 2025), Berton method (Berton, 2021) Maekawa method (copied shielding factors from STCA) (Maekawa, 1968)
Certification Noise Levels modules • Perceived noise level, tone corrected (PNLT) • Effective perceived noise level (EPNL)	ICAO Annex 16 Volume I: Aircraft noise App. 2-13 (ICAO, 2017) ICAO Annex 16 Volume I: Aircraft noise App. 2-13 (ICAO, 2017)

Berton, J. (2021, August 2-6). *Simultaneous use of ground reflection and lateral attenuation noise models* [Conference presentation]. AIAA AVIATION 2021 FORUM, virtual. https://doi.org/10.2514/6.2021-2214

Chien, C., & Soroka, W. (1975). Sound propagation along an impedance plane, *Journal of Sound and Vibration*, 43(1), 9–20.

Emmerling, J., Kazin, S., & Matta, R. (1976). *Core engine noise program Volume III. Prediction methods – Supplement I: Extension of prediction methods, technical report*. Ohio Aircraft Engine Business Group, General Electric Co., Cincinnati, Ohio. https://apps.dtic.mil/sti/pdfs/ADA030376.pdf

Fink, M. R. (1977). *Airframe noise prediction method*. United Technologies Research Center, East Hartford, Connecticut.

Golub, R., Rawls Jr, J. W., & Yeager, J. C. (2004). *High Speed Research Noise Prediction Code (HSRNOISE) user's and theoretical manual*. NASA. https://ntrs.nasa.gov/api/citations/20040200978/downloads/20040200978.pdf

Heidmann, M. F. (1979). *Interim prediction method for fan and compressor source noise* (NASA-TM-x71763). NASA. ntrs.nasa.gov/api/citations/19750017876/downloads/19750017876.pdf

Hough, J. W., & Weir, D. S. (1996). *Aircraft noise prediction program (ANOPP) fan noise prediction for small engines* (NASA-CR-198300). NASA Langley Research Center. ntrs.nasa.gov/api/citations/19960042711/downloads/19960042711.pdf

ICAO. (2017). *Annex 16 to the Convention on International Civil Aviation Environmental Protection Volume 1: aircraft noise* (Ed. 8). International Civil Aviation Organization (ICAO).

Kontos, K. B., Janardan, B., & Gliebe, P. (1996a). *Improved NASA-ANOPP noise prediction computer code for advanced subsonic propulsion systems, Volume 1: ANOPP evaluation and fan noise model improvement* (NASA CR-195480). NASA Lewis Research Center. https://ntrs.nasa.gov/api/citations/19960048499/downloads/19960048499.pdf

Kontos, K. B., Kraft, R. E., & Gliebe, P. R. (1996b). *Improved NASA-ANOPP noise prediction computer code for advanced subsonic propulsion systems, Volume 2: Fan suppression model development* (NASA-CR-202309). NASA Lewis Research Center. https://ntrs.nasa.gov/api/citations/19960048499/downloads/19960048499.pdf

Maekawa, Z. (1968). Noise reduction by screens, *Applied Acoustics*, 1(3), 157–173.

Montegani, F. J. (1979). Computation of atmospheric attenuation of sound for fractional-octave bands (NASA Technical Paper 1412). NASA. ntrs.nasa.gov/api/citations/19790009488/downloads/19790009488.pdf

SAE International. (2025). AIR5662: *Method for predicting lateral attenuation of airplane noise*. https://doi.org/10.4271/AIR5662

SAE International. (2021). *ARP-876F: Gas turbine jet exhaust noise prediction*. https://doi.org/10.4271/ARP876F

The *Geometry* component computes geometrical variables related to the aircraft trajectory relative to the observer position, x_{obs}, i.e., source-observer distance, r; polar and azimuthal directivity angle, (θ, ϕ); elevation angle, β; and observer time, t_O. In the *Source and Suppression* modules, the mean-square acoustic pressure of the different noise sources is computed, and noise suppression is applied to the fan and airframe mean-square acoustic pressure, for the fan liner treatment and the SST airframe calibration, respectively. In the *Propagation* component, the source mean-square acoustic pressure is propagated to the observer through the atmosphere, using the propagation effects listed in Table 2. Finally, the noise levels at the observer, including overall sound pressure level (SPL), tone-corrected perceived noise level (PNLT), and EPNL, are computed in the *Levels* and *Integrated Levels* components.

The Jacobian of the individual noise modules in Table 2 are computed using an AD method. AD provides more accurate derivative computations compared to finite-difference (FD) methods, as well as faster computations compared to FD and complex-step (CS) differentiation methods. The Julia ForwardDiff package (Revels et al., 2016) is used to implement the partial derivatives of the aircraft noise estimation model.

Milestones

- Developed a chemical reactor network–based combustor model, and calibrated NO_x and carbon monoxide (CO) emissions to the EEDB data using combustor inlet values obtained from the NPSS model of the CFM56-5B engine.
- Developed an open-source aircraft noise estimation model estimating the static noise database from relevant engine parameters, the static-to-flight noise projection, and the certification noise levels.
- Provided the sensitivities of the certification noise levels to engine operating parameters by the model to enable multi-disciplinary design optimization and optimal control.

Major Accomplishments

Emissions Model

A framework was developed to estimate the NO_x and CO emissions indices of the donor engine, given the relevant engine parameters using a reactor network model. A comparison of the model developed and the EEDB data is shown in Figure 13. The derivative and clean-sheet engine analyzed in the work described here assumes that the combustor technology used is similar to that of the donor engine and therefore the calibrated parameters are assumed to hold for the clean-sheet engine as well. A soot model to estimate the non-volatile particulate matter (nvPM) concentrations is currently being integrated into the combustor model.

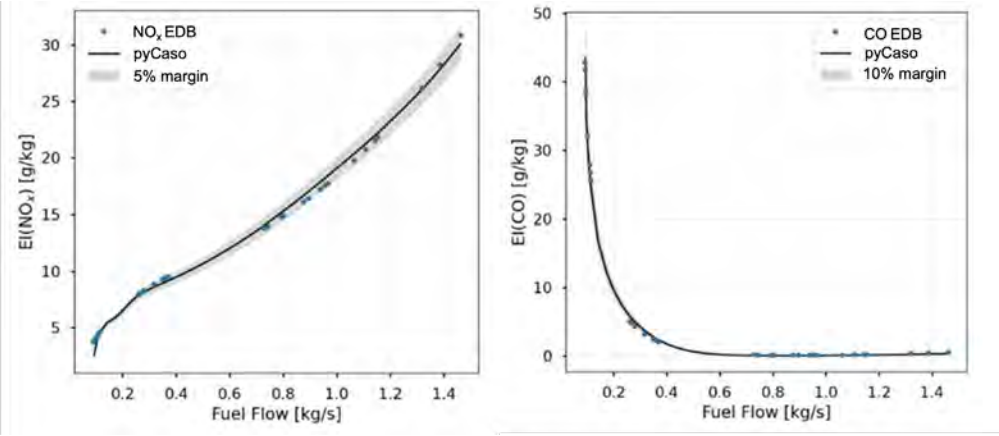

Figure 15. Comparison of NO_x emission indices (left) and CO emission indices (right) of the combustor model and ICAO data from the EEDB.

Aircraft Noise Model (pyNA)

A framework was set up to estimate the noise levels (i.e., SPL, PNLT and EPNL) of the engine given the relevant engine parameters using a semi-empirical model.

Aircraft Noise Estimation Model: Verification

The utility of the aircraft noise model is evaluated based on the noise assessment of the STCA, designed by NASA to evaluate environmental and economic impacts of SST (Berton et al., 2020). The noise modules are evaluated on the standard take-off trajectory, denoted by Berton et al. (2018) as a trajectory that abides by the noise regulation procedures in ICAO Annex 16 for subsonic transport-category airplanes (Berton et al., 2018; ICAO, 2017a). The STCA is a 55-tonne, 8-passenger, Mach 1.4 business tri-jet, cruising at altitudes between 12.5 and 15.5 km (Berton et al., 2020). The STCA noise assessment was performed by Berton et al. (2018) using the NASA Aircraft Noise Prediction Program (ANOPP) (Zorumski, 1982).

The spectral and polar directivity SPL-distribution the fan inlet and discharge, core, jet mixing, and airframe source modules are determined at the zenith point of the flyover observer for a series of one-third octave frequencies, as shown in the polar plots in Figure 14. The engine noise sources are independent of the azimuthal directivity angle, ϕ; the airframe noise source module is plotted for an azimuthal directivity angle, ϕ = 0 deg. The SPL distribution is computed along a circular arc with a 0.3048 m (1 ft) radius from the noise source. The SPL distributions are compared to the NASA STCA ANOPP noise assessment in the polar plots of Figure 14. Excellent agreement is found – a root mean square (RMS) error <0.1dB across polar directivity angles and frequencies – between the current noise model (pyNA) and STCA data for the core, jet mixing and airframe source SPL. Good agreement is found – an RMS error <1.3dB – for the fan inlet and discharge broadband component, although discrepancies can be found in the fan tonal components of the fan inlet and discharge noise.

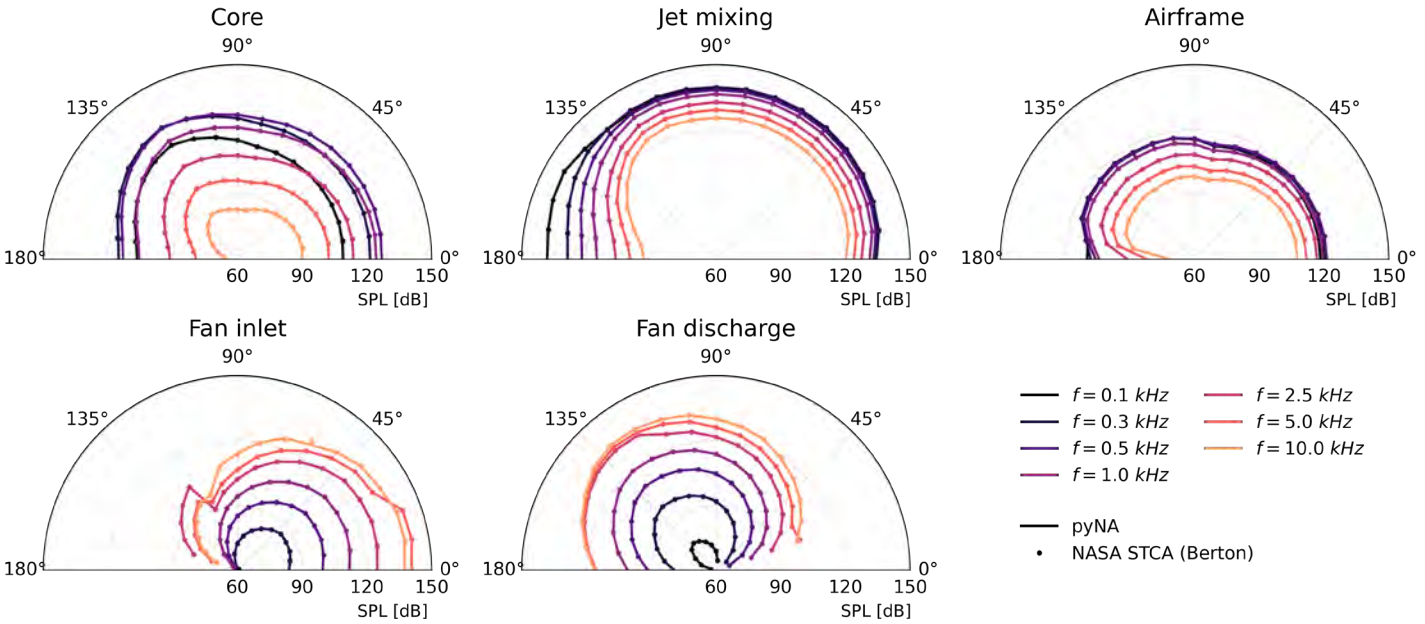

Figure 16. Comparison of the spectral and directional sound pressure level (SPL) distribution at the zenith point of the flyover microphone determined using the current noise model (pyNA) and NASA ANOPP (Berton et al., 2018).

The total PNLT at the lateral and flyover microphones computed by the current noise model (pyNA) is compared to the NASA STCA ANOPP noise assessment in Figure 15. The PNLT curves computed by pyNA have an RMS error of 0.35 PNdB in the domain of dependence of the EPNL, compared to those computed by ANOPP.

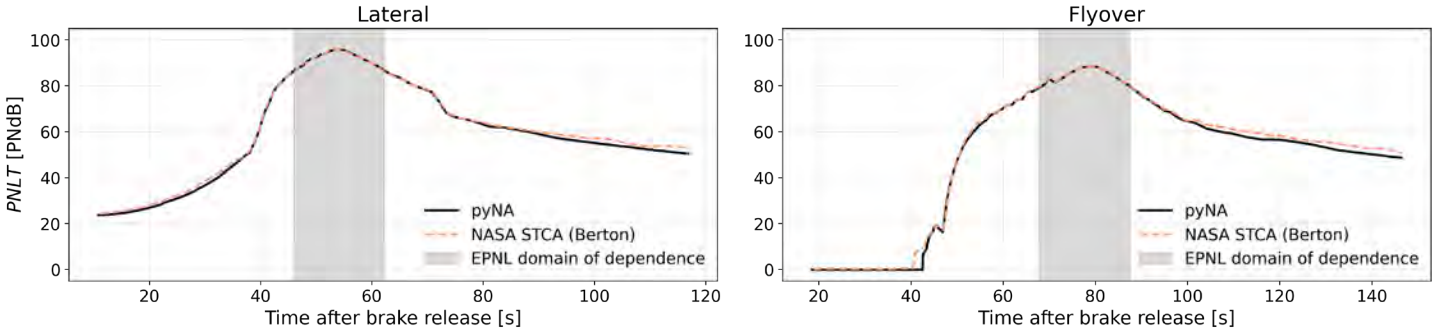

Figure 17. Comparison of the tone-corrected perceived noise level (PNLT) at the lateral (left) and flyover (right) microphone determined using the current noise model (pyNA) and NASA ANOPP (Berton et al., 2018).

The EPNL for individual noise sources and total EPNL are compared to the NASA STCA ANOPP noise assessment in Table 3. A maximum difference across all noise sources of -1.4 EPNdB is found for fan inlet noise source module. This difference is considered acceptable as the fan inlet noise is neither the dominating noise source for the lateral nor the flyover microphone. For the total EPNL, a maximum difference of -0.1 EPNdB is found for the flyover microphone, set mostly by the good agreement for the jet mixing noise source module.

Table 3. Comparison of the individual noise source and total EPNL determined using the current noise model (pyNA) and NASA ANOPP (Berton et al., 2018). The lateral microphone position is assumed to be at the x-location where the aircraft reaches 304.8 m (1000 ft) altitude, i.e., $x_{lateral}$ = 3756 m.

Noise source	Lateral microphone [EPNdB]			Flyover microphone [EPNdB]		
	pyNA	STCA	Δ	pyNA	STCA	Δ
Fan inlet	50.4	49.5	+0.9	35.6	37.0	-1.4
Fan discharge	77.0	76.9	+0.1	71.8	71.8	0.0
Combustor	76.9	77.0	-0.1	73.3	73.6	-0.3
Jet mixing	94.6	94.6	0.0	87.8	87.9	-0.1
Airframe	62.0	-*	-*	64.7	64.8	-0.1
Total	**95.0**	**95.0**	**+0.0**	**88.5**	**88.6**	**-0.1**

*The NASA STCA results for airframe noise source were not available at the lateral microphone.

Sensitivities of noise levels to engine operating variables

The aircraft noise estimation model provides sensitivities of acoustic objective functions with respect to engine operating variables to enable multi-disciplinary design optimization and optimal control. Figure 16 shows the sensitivities of the EPNL at the lateral and flyover microphone with respect to key engine operating variables driving the aircraft noise signature. From Figure 16 it can be seen that noise levels are dominantly sensitive to the jet velocity, as is expected from high specific thrust engines for SST.

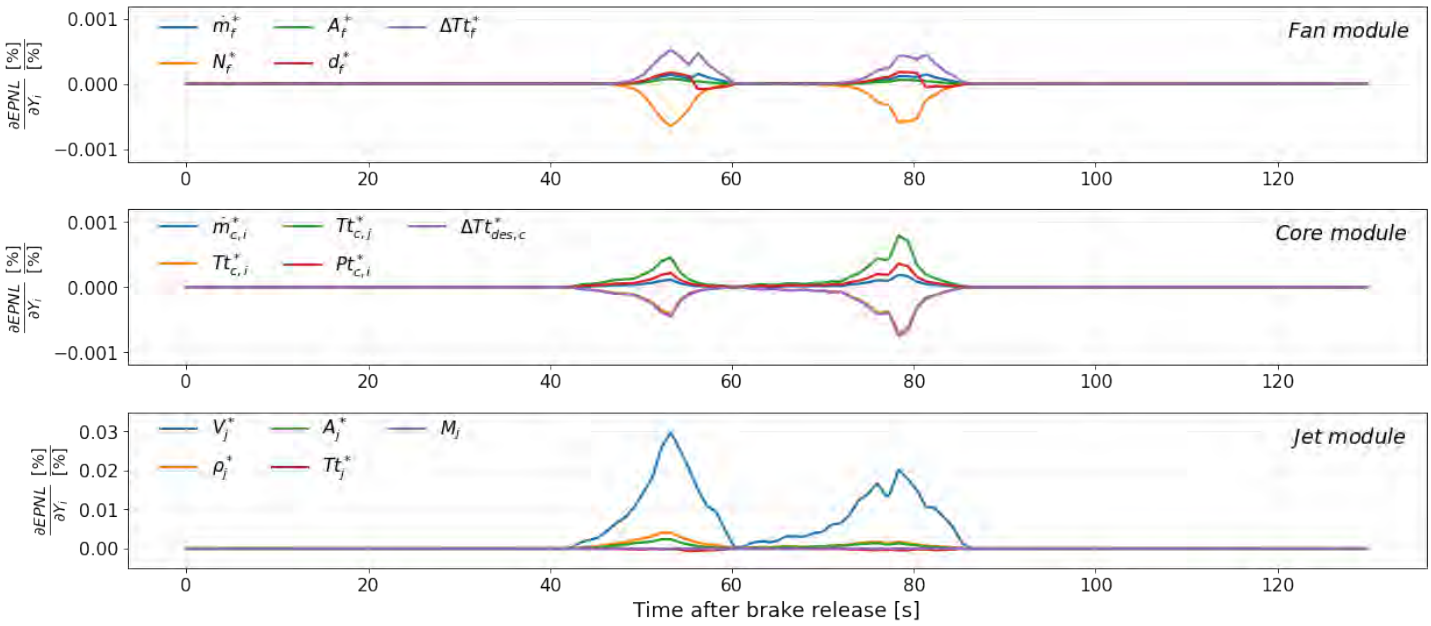

Figure 18. Sensitivities of EPNL along NASA STCA standard take-off trajectory with respect to engine operating variables including the fan (top), core (middle), jet (bottom) for the lateral and flyover microphone.

Sensitivities of Noise Levels to Engine Design Variables

The sensitivities of the environmental performance metrics of a clean-sheet engine with respect to a set of engine design variables are assessed for the NASA STCA business jet. The sensitivities of the environmental performance metrics to engine design variables, $\frac{\partial Y_{env}}{\partial X_{des}}$, are normalized, i.e., $\frac{\partial Y_{env}}{\partial X_{des}}|_{norm} = \frac{\partial Y_{env}}{\partial X_{des}} \cdot \frac{X_{des}}{Y_{env}}$. The normalized sensitivities are given in units of [%]/[%], also known as [pts]. These sensitivities give insight into the design trades of new engine designs configurations during the preliminary design process. The impact of the derivative engine design space constraints imposed by a donor core on the engine environmental performance is briefly considered.

The sensitivities of the environmental performance metrics to engine design variables of the clean-sheet engine without fan size constraint are shown in Table Table 4. The effect of the change in design variables on the fan size is shown in Table 5.

Table 4. Sensitivity of environmental performance metrics with respect to engine design parameters ([%]/[%]). The environmental performance metrics are found to be most sensitive to the fan pressure ratio, π_{fan}.

Environmental Performance Metric	π_{fan}	π_{HPC}	$T_{t,4}/T_{t,2}$	ER_{mix}
Take-off effective perceived noise level, $EPNL_{TO}$	+0.198	-0.019	-0.020	+0.080
Top of climb thrust-specific fuel consumption, $TSFC_{TOC}$	+0.165	-0.114	-0.063	+0.117
Cruise thrust-specific fuel consumption, $TSFC_{cruise}$	-0.040	-0.097	-0.059	+0.013
Take-off NO_x emission index, $EI(NO_x)_{TO}$	+1.978	+1.257	-0.066	+0.259
Cruise NO_x emission index, $EI(NO_x)_{cruise}$	+1.638	+1.786	-0.026	-0.106

Table 5. Sensitivity of fan diameter with respect to engine design parameters ([%]/[%]).

Environmental Performance Metric	π_{fan}	π_{HPC}	$T_{t,4}/T_{t,2}$	ER_{mix}
Fan diameter, d_{fan}	-0.750	+0.063	+0.057	-0.295

From Table 4, it can be seen that the take-off EPNL is most sensitive to the design fan pressure ratio, π_{fan}. The increase in design fan pressure ratio causes an increase in mixed jet velocity and thus, for a given thrust-requirement, reduces the fan size, as shown in Table 5. A similar effect happens for the mixer extraction ratio, ER_{mix}. The increase in jet velocity caused by the increase in fan pressure ratio is the dominant driver of the increased take-off noise levels. Furthermore, from all design variables, the fan diameter is found to have the highest sensitivity to the design fan pressure ratio. This behavior is well-known for subsonic transport engines.

The sensitivity of the take-off noise levels to the engine core design variables, i.e., π_{HPC} and $T_{t,4}/T_{t,2}$, is significantly smaller (factor of 10) compared to that of the design fan pressure ratio. This also shows that, even if the core design variables were constrained by the donor core of a derivative engine design, the impact of such constraints would be relatively small as the take-off noise levels are mainly sensitive to design fan pressure ratio. The low-spool of the derivative engine is purpose-designed to meet the propulsion system requirements. This is unlike the cruise thrust-specific fuel consumption and the take-off NO_x emission index, where the sensitivities to the HPC pressure ratio are of the same order of magnitude as those of the design fan pressure ratio.

At the engine design point, i.e., the top of climb operating point, the sensitivity of thrust-specific fuel consumption (TSFC) with respect to fan pressure ratio is positive, governed by the decrease in propulsive efficiency at higher fan pressure ratios. The sensitivity with respect to HPC pressure ratio and $T_{t,4}/T_{t,2}$ is negative, driven by an increase in thermal efficiency. At the cruise operating point, the sensitivity of TSFC with respect to fan pressure becomes negative due to off-design effects.

At the take-off and cruise operating point, the dominant sensitivities of the NO_x emissions are those with respect to the fan and HPC pressure ratio. Both sensitivities are positive since an increase in the fan and HPC pressure ratios cause an increase in the overall pressure ratio (OPR) resulting in higher $T_t,3$ and $P_t,3$, and thus higher NO_x emissions.

Finally, increasing the HPC pressure ratio for a fixed $T_{t,4}/T_{t,2}$ and ER_{mix} results in a lower total temperature at the HPT exit. Consequently, the mixed jet velocity is lower and therefore, to meet the engine thrust requirement, the engine mass flow will and necessary fan size increases. This results in a positive sensitivity $\partial d_{fan}/\partial \pi_{HPC}$. An increase in $T_{t,4}/T_{t,2}$ at a fixed ER_{mix} similarly results in lower mixed jet velocity, thus increasing the necessary fan size. The sensitivity $\partial d_{fan}/\partial(T_{t,4}/T_{t,2})$ is thus also expected to be positive.

The sensitivities of the environmental performance metrics to engine design variables of the clean-sheet engine with fan size constraint are shown in Table 6.

Table 6. Sensitivity of environmental performance metrics with respect to engine design parameters ([%]/[%]). A constrained fan size results in limited sensitivity of the take-off noise levels with respect to engine design variables.

Environmental performance metric	π_{fan}	π_{HPC}	$T_{t,4}/T_{t,2}$
Take-off effective perceived noise level, $EPNL_{TO}$	-0.007	-0.002	-0.005
Top of climb thrust-specific fuel consumption, $TSFC_{TOC}$	-0.134	-0.088	-0.041
Cruise thrust-specific fuel consumption, $TSFC_{cruise}$	-0.074	-0.094	-0.057
Take-off NO_x emission index, $EI(NO_x)_{TO}$	+1.319	+1.313	-0.016
Cruise NO_x emission index, $EI(NO_x)_{cruise}$	+1.907	+1.763	-0.046

Compared to the results in Table 4, the additional fan size constraint causes the sensitivity of the take-off EPNL with fan pressure ratio, π_{fan}, to become equally insignificant as the sensitivities to the engine core design variables. Since the fan

size and fan face Mach number are fixed, the mass flow through the engine is also fixed. Therefore, the necessary jet velocity to meet the required thrust demand is fixed, resulting in approximately constant take-off noise levels. This effect is specific to high specific thrust engines for SST, having a noise signature dominated by jet noise.

As can be seen from Table 6, the cruise thrust-specific fuel consumption and the take-off NO_x emission index can still be traded by varying the three design variables (π_{fan}, π_{HPC}, and T_{t4}/T_{t2}). The sensitivities of TSFC with respect to all design variables in Table 6 are negative; an increase in both fan and HPC pressure ratios as well as T_{t4}/T_{t2} results in an increase in engine thermal efficiency. The effect of the fan pressure ratio on the propulsive efficiency is now limited because of the constraint fan size. The sign of the sensitivities of engine NO_x emissions with respect to the set of design variables do not change when adding a fan size constraint.

Publications

Voet, L., Speth, R., Sabnis, J., Tan, C., & Barrett, S. (2022). Sensitivities of aircraft acoustic metrics to engine design variables for multi-disciplinary optimization. *AIAA Journal*, *60*(8). https://doi.org/10.2514/1.J061411

Outreach Efforts

- Dr. Jayant Sabnis gave a presentation titled "Noise and emission characteristics of commercial supersonic aircraft propulsion systems" at the Aviation Noise and Emissions Symposium on March 5, 2019.
- Prof. Steven Barrett gave a presentation titled "Clean-sheet supersonic engine design and performance" at the ASCENT meeting in Atlanta, GA, on April 19, 2019.
- Dr. Jayant Sabnis gave a presentation titled "Clean-sheet supersonic engine design and performance" at the ASCENT meeting in Alexandria, VA, on October 22, 2019.
- Mr. Prashanth Prakash and Mr. Laurens Voet gave a presentation titled "Clean-sheet supersonic engine design and performance" at the at the virtual ASCENT meeting on September 30, 2020.

Awards

- Mr. Laurens Voet, 2021, AIAA 2021 Luis de Florez Graduate Award

Student Involvement

This task was conducted primarily by Prashanth Prakash and Laurens Voet, graduate research assistants working under the supervision of Dr. Jayant Sabnis, Dr. Raymond Speth, and Dr. Choon Tan.

References

Berton, J. (2021, August 2-6). *Simultaneous use of ground reflection and lateral attenuation noise models* [Conference presentation]. AIAA AVIATION 2021 FORUM, virtual. https://doi.org/10.2514/6.2021-2214

Berton, J. J., Huff, D. L., Geiselhart, K., & Seidel, J. (2020, January 6–10). *Supersonic technology concept aeroplane for environmental studies* [Conference presentation]. AIAA Scitech 2020 Forum, Orlando, Florida.

Berton, J., Jones, S. M., Seidel, J. A., & Huff, D. L. (2018). Noise predictions for a supersonic business jet using advanced take-off procedures. *Aeronautical Journal, 122*(1250), 556–571. http://dx.doi.org/10.1017/aer.2018.6

Chien, C., & Soroka, W. (1975). Sound propagation along an impedance plane, *Journal of Sound and Vibration*, 43(1), 9–20.

Emmerling, J., Kazin, S., & Matta, R. (1976). *Core engine noise program Volume III. Prediction methods – Supplement I: Extension of prediction methods, technical report*. Ohio Aircraft Engine Business Group, General Electric Co., Cincinnati, Ohio. https://apps.dtic.mil/sti/pdfs/ADA030376.pdf

Fink, M. R. (1977). *Airframe noise prediction method*. United Technologies Research Center, East Hartford, Connecticut.

Golub, R., Rawls Jr, J. W., & Yeager, J. C. (2004). *High Speed Research Noise Prediction Code (HSRNOISE) User's and Theoretical Manual*. NASA. https://ntrs.nasa.gov/api/citations/20040200978/downloads/20040200978.pdf

Gray, J. S., Hwang, J. T., Martins, J. R., Moore, K. T., & Naylor, B. A. (2019). OpenMDAO: An open-source framework for multidisciplinary analysis and optimization. *Structural and Multidisciplinary Optimization, 59*(4), 1075–1104.

Heidmann, M. F. (1979). *Interim prediction method for fan and compressor source noise* (NASA-TM-x71763). NASA. ntrs.nasa.gov/api/citations/19750017876/downloads/19750017876.pdf

Hough, J. W., & Weir, D. S. (1996). *Aircraft noise prediction program (ANOPP) fan noise prediction for small engines* (NASA-CR-198300). NASA Langley Research Center. ntrs.nasa.gov/api/citations/19960042711/downloads/19960042711.pdf

ICAO. (2017a). *Annex 16 to the Convention on International Civil Aviation Environmental Protection Volume 1: aircraft noise* (8th Ed). International Civil Aviation Organization (ICAO).
ICAO. (2017b). *Annex 16 environmental protection. Volume II: Aircraft engine emissions* (4th Ed). International Civil Aviation Organization (ICAO).
Kontos, K. B., Janardan, B., & Gliebe, P. (1996a). *Improved NASA-ANOPP noise prediction computer code for advanced subsonic propulsion systems, Volume 1: ANOPP evaluation and fan noise model improvement* (NASA CR-195480). NASA Lewis Research Center. https://ntrs.nasa.gov/api/citations/19960048499/downloads/19960048499.pdf
Kontos, K. B., Kraft, R. E., & Gliebe, P. R. (1996b). *Improved NASA-ANOPP noise prediction computer code for advanced subsonic propulsion systems, Volume 2: Fan suppression model development* (NASA-CR-202309). NASA Lewis Research Center. https://ntrs.nasa.gov/api/citations/19960048499/downloads/19960048499.pdf
Lambe, A.B., & Martins, J. R. R. A. (2012). Extensions to the design structure matrix for the description of multidisciplinary design, analysis, and optimization processes. *Structural and Multidisciplinary Optimization, 46*(2). 273–284. https://doi.org/10.1007/s00158-012-0763-y
Maekawa, Z. (1968). Noise reduction by screens, *Applied Acoustics*, 1(3), 157–173.
Montegani, F. J. (1979). Computation of atmospheric attenuation of sound for fractional- octave bands (NASA Technical Paper 1412). NASA. ntrs.nasa.gov/api/citations/19790009488/downloads/19790009488.pdf
Revels, J., Lubin, M., & Papamarkou, T. (2016). *Forward-mode automatic differentiation in Julia*. Cornell University, arXiv:1607.07892. https://doi.org/10.48550/arXiv.1607.07892
SAE International. (2021). *ARP-876F: Gas turbine jet exhaust noise prediction*. https://doi.org/10.4271/ARP876F
SAE International. (2025). AIR5662: Method for predicting lateral attenuation of airplane noise. https://doi.org/10.4271/AIR5662
Zorumski, W. E. (1982). *Aircraft noise prediction program theoretical manual part 1-2, technical report*. NASA.

Task 4 - Evaluate the Impact of Improved Technology on Relative Performance Benefits of Clean-Sheet and Derivative Engines

Massachusetts Institute of Technology

Objective

The objective of this first task is to quantify the impact that improvements in technology will have on the relative performance of clean-sheet engine designs over derivative designs. Specifically, we consider the impact of technology improvements in the turbomachinery design, turbine material, cooling technology, and combustor design for low NO_x emissions for the STCA developed by NASA (Berton & Geiselhart, 2019).

Research Approach

We parameterize the technology level of various components as follows:

- **Turbomachinery**
  The technology level of the turbomachinery components (i.e., fan, compressor, and turbines) is quantified by the polytropic efficiency (η_p) of the components.

- **Turbine Material and Cooling Technology**
  The turbine material limits, such as advanced ceramic matrix composites, thermal barrier coatings, and cooling technology, are quantified by the metal temperature that the turbine vanes and blades are allowed to reach (T_{vane} and T_{blade}, respectively).

- **Combustor Technology**
  The design space benefits of a clean-sheet engine design would be more readily accessible if the emissions of NO_x were reduced by using a more advanced combustor model. The combustor technology can be parameterized by using a previously developed reactor network model.

Milestones

- Developed and used a parametrized representation of the technology level of various components to evaluate the impact of improved technology on the performance of clean-sheet and derivative engines.

Major Accomplishments

The sensitivity of the thrust specific fuel consumption to the technology levels of the turbomachinery, turbine material, and cooling were calculated for both clean-sheet and derivative engines. Figure 17 shows that the derivative engine benefits from a 0.33% and 0.46% improvement in SFC per percentage-point improvement in the polytropic efficiency of the LPT and fan, respectively. These sensitivities are calculated for an optimal engine, sized for a fixed propulsion system requirement (on the basis of the thrust requirement of the STCA). Specifically, each point on the graph represents an engine optimized for minimum SFC with the constraints outlined in the previous section. Because the derivative engine uses the donor core, only the fan and LPT can be designed by using the improved technology.

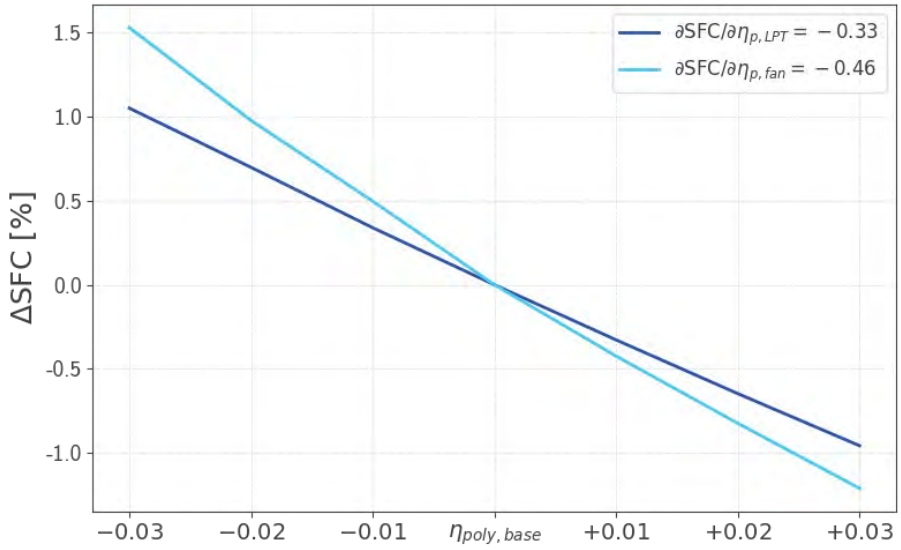

Figure 19. Sensitivity of a derivative engine SFC to the polytropic efficiency of the low-pressure spool components (LPT and fan).

The sensitivities of the clean-sheet engine are different from those of the derivative engine because the core of the engine can be redesigned to obtain an optimal SFC engine at each point. Because the high-pressure spool of the clean-sheet engine is designed, we also calculated the sensitivity of SFC to the polytropic efficiency of the HPC and HPT in addition to the low-pressure spool components, as shown in Figure 18.

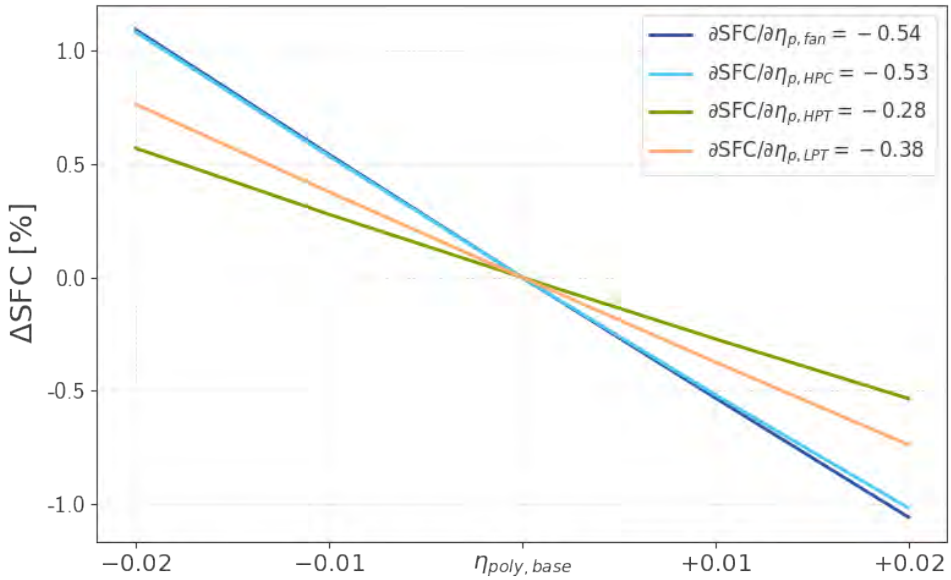

Figure 20. Sensitivity of clean-sheet engine SFC to the polytropic efficiency of the turbomachinery.

For a clean-sheet engine design, the pressure ratio of the engine is limited not by the material limits of the last stage of the HPC but by the imposed constraint on the emission index of NO_x. We found that a 1% increase in the allowable turbine metal temperature results in a 0.25% decrease in the clean-sheet engine SFC.

The cumulative effects of improvements on each of the above engine components are shown for both the derivative and clean-sheet engine in Figure 19. Table 7 shows the assumed magnitude of improvement to the engine components. Improvements in the low-pressure spool and low-NO_x combustor designs have the largest benefit in clean-sheet engine SFC. The clean-sheet engine with advanced technology has a 4.1% lower SFC than the derivative engine with advanced low-pressure spool components.

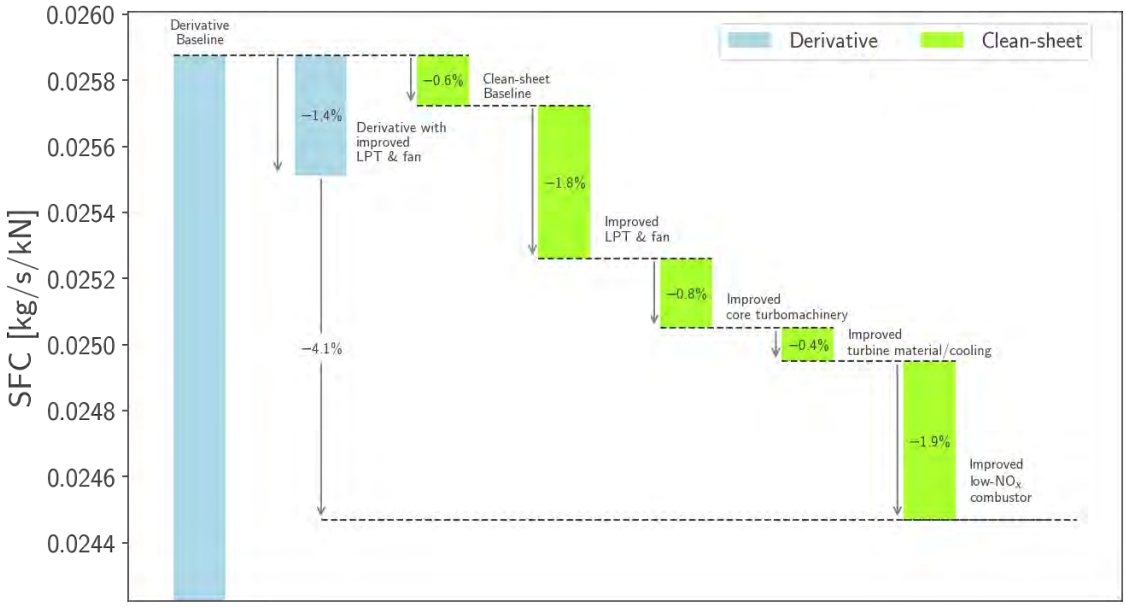

Figure 21. Impact of technology improvements on the SFC of derivative and clean-sheet engines for the STCA.

Table 7. Assumed magnitude of technology improvements for clean-sheet and derivative engines.

Components	Derivative engine	Clean-sheet engine
$\Delta\eta_p$ of low-pressure spool turbomachinery	+0.02	+0.02
$\Delta\eta_p$ of high-pressure spool turbomachinery	-	+0.01
$\Delta T_{metal,HPT}$	-	+100 K
Emission index of NO_x	-	Improved low-NO_x combustor modelled on the PW1133G TALON-X combustor

Publications
None.

Outreach Efforts
- Presented at the ASCENT Advisory Committee Spring Meeting (April 5–7, 2022).
- Presented at the Aviation Emissions Characterization Roadmap Annual Meeting (May 24–26, 2022).

Awards
None.

Student Involvement
This work was performed primarily by graduate research assistant Prashanth Prakash working under the supervision of Dr. Jayant Sabnis, Dr. Raymond Speth, and Dr. Choon Tan.

References

Berton, J., & Geiselhart, K. (2019). *NASA 55 tonne Supersonic Transport Concept Aeroplane (STCA) release package*. NASA Glenn Research Center & NASA Langley Research Center.

Task 5 – Evaluate the Effects of Fan Diameter and Unconventional Architectures on the Environmental Impacts of Clean-Sheet Engines

Massachusetts Institute of Technology

Objective

The objective of this task is to quantify the effects of fan diameter constraints and use of unconventional engine architectures on the emissions of clean-sheet engines. In particular, we examine the combined impact of the following cases:

- Effect of fan diameter on supersonic drag sources, and subsequent impacts on thrust requirements and engine performance.
- Use of hybrid-electric systems powered primarily with conventional fuel alongside a battery-based supplement used during LTO flight.

The work presented is done for the airframe and mission of the STCA developed by NASA (Berton et al., 2020).

Research Approach

The NPSS software (Claus et al., 1991) was chosen for analysis of engine performance and emissions. Because it is an industry-standard tool, it facilitates future collaboration with the broad user base. The clean-sheet engine cycle deck from Prashanth et al. (2023) is used to obtain a baseline design.

Supersonic Drag Sources

Supersonic drag forces on an engine fall primarily into three categories: (1) bypass drag, (2) spillage drag, and (3) wave drag. Bypass and spillage drag represent losses due to off-design operation of a supersonic inlet. In this work, engine inlets are assumed to be operated on-design or to contain variable-geometry components to maintain well-matched operation across the mission. Therefore, we assume that the contributions of spillage and bypass drag are negligible. The effects of such systems (weight, complexity, etc.) are not considered here.

The Fraenkel model for external cowl drag on open-nosed bodies of revolution (as presented by Seddon and Goldsmith [1999]) is used to model the remaining supersonic drag source, wave drag. The aspect ratio of the inlet cross-section (radius/length) is taken to be constant and equal to the value for the existing STCA engine. Fan diameter is used as a proxy for maximum inlet radius and is allowed to vary. A conical profile is conservatively used to minimize drag.

Although the exact value of the wave drag due to the engine inlet cowls on the baseline aircraft is unknown, it can be estimated with the above model. Consequently, the difference in wave drag can be estimated for a clean-sheet engine with a specified fan diameter relative to the baseline design. This difference is then used alongside steady flight assumptions to obtain the difference in thrust requirement relative to the baseline mission presented in Berton et al. (2020).

Previous Hybrid-Electric Assessments

Before implementing a full hybrid-electric NPSS engine model, we first qualitatively assessed the potential benefits of hybrid electrification. We assume an architecture wherein electric systems are used only during the LTO phase of flight, when the greatest demand is placed on the engine. Consequently, the gas turbine component of the engine can be sized more closely to cruise requirements. Similar analyses in subsonic systems (Kang et al., 2022; Lammen & Vankan, 2020; Lents et al., 2016; Seitz et al., 2018) suggest specific fuel consumption benefits on the order of 5%, alongside minor improvements to NO_x emissions. These benefits are hypothesized to manifest through three primary mechanisms:

- Lower peak gas turbine corrected fan speed requirement: This aspect could allow the gas turbine to operate closer to the design condition (100% corrected speed) during cruise, improving component efficiency.
- Lower peak engine turbine-entry-temperature (TET): If the maximum TET point occurs during LTO, electric systems could be used to reduce the TET required by the gas turbine, thereby potentially improving NO_x emissions and propulsive efficiency.

- Lower thrust requirements at pinch points: Electric systems could be used to reduce the thrust requirements of the gas turbine at the pinch points of the mission, thereby allowing the engine to be sized more closely to cruise thrust requirements.

The final mechanism, thrust requirement, was implemented indirectly to maintain the known mission profile. The time in the mission at which a given constraint is placed was varied, and the altitude, Mach number, and thrust requirement could then be calculated at that new time. As an example, the thrust pinch point occurs at 27 kft at a Mach number of 0.85. In a hybrid-electric engine, the gas turbine would not be able to produce sufficient thrust at that point alone and would require assistance by the electric systems. To model this scenario while maintaining the STCA mission profile, the engine is sized for thrust at a slightly later (positive time deviation) or slightly earlier (negative time deviation) mission point. An engine sized for thrust at either of these points will not produce sufficient thrust at the actual thrust pinch point but may be sized more optimally for cruise. This procedure of varying the time at which a thrust constraint is applied is repeated for other key points in the mission.

To test these mechanisms, NPSS is used to examine the sensitivity of emissions metrics to the corrected fan speed, turbine inlet temperature, and thrust requirement (with time as a proxy) at several points in the STCA LTO profile. These points are the thrust pinch point (27 kft., Mach 0.85), the thermal pinch point (42 kft., Mach 1.4), and the aerodynamic design point (ADP); 41 kft., Mach 1.4). Emissions are then evaluated at the beginning of cruise point (44 kft., Mach 1.4) as an estimate of overall cruise emissions.

Major Accomplishments

Supersonic Drag Implementation

The wave drag was first estimated for several supersonic regime Mach numbers for the original STCA engine design. The fan diameter (D_f) was then allowed to vary. The percentage deviation in engine cowl drag area (C_dA) from the baseline STCA design is shown in Figure 20 as a function of Mach number. The drag area of an engine cowl monotonically increases with a local sensitivity of $\partial C_dA/\partial D_f = 3.5$. The drag area relative to the baseline STCA was found to have minimal variation due to the Mach number. At a fixed fan diameter, the change in drag area was between 1.6% at -10% fan diameter and 3.3% at $+10\%$ fan diameter. Notably, the effect of Mach number grows with increasing fan diameter, thus indicating that this effect would need to be accounted for at high fan diameters.

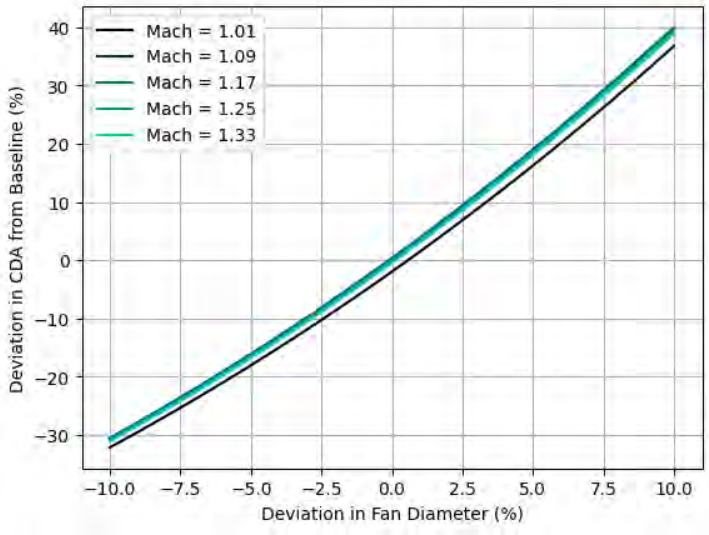

Figure 22. Effect of fan diameter variation on engine external cowl drag area (CDA), as a function of Mach number.

Sensitivities

The supersonic drag model described above was implemented into the NPSS clean-sheet cycle deck, and sensitivities of specific air range (SAR), TSFC, and fan diameter were calculated due to variation in TET, corrected fan speed, and thrust (with time as a proxy). The resulting sensitivities are generally non-linear (Figure 21). Variations in emissions metrics and fan diameter due to turbine inlet temperature have negligible dependence on the point at which the temperature was prescribed, thus suggesting strong correlations between temperature changes at all tested points. We see improved SAR and SFC for increasing turbine inlet temperature, to maxima on the order of 0.5%. SFC was minimized with a corrected fan speed deviation of -5% for all three points of interest. While SAR exhibits a maximum, the value of that maximum is decreased, because of the resultant increase in fan diameter and thus drag.

The emissions and fan diameter sensitivities due to sizing time variation are not smooth, because variations in time equate to variations in altitude, Mach number, and thrust, in accordance with the prescribed LTO mission profile. As such, when an inflection point of the mission (e.g., end of climb) is reached, the behavior of the mission parameters with respect to time changes suddenly. From the time sensitivities, we see SAR and SFC benefits resulting from a positive deviation of time at the thrust pinch point. This finding indicates that sizing the engine thrust to a later point in the mission and producing insufficient thrust at the actual pinch point does improve cruise emissions.

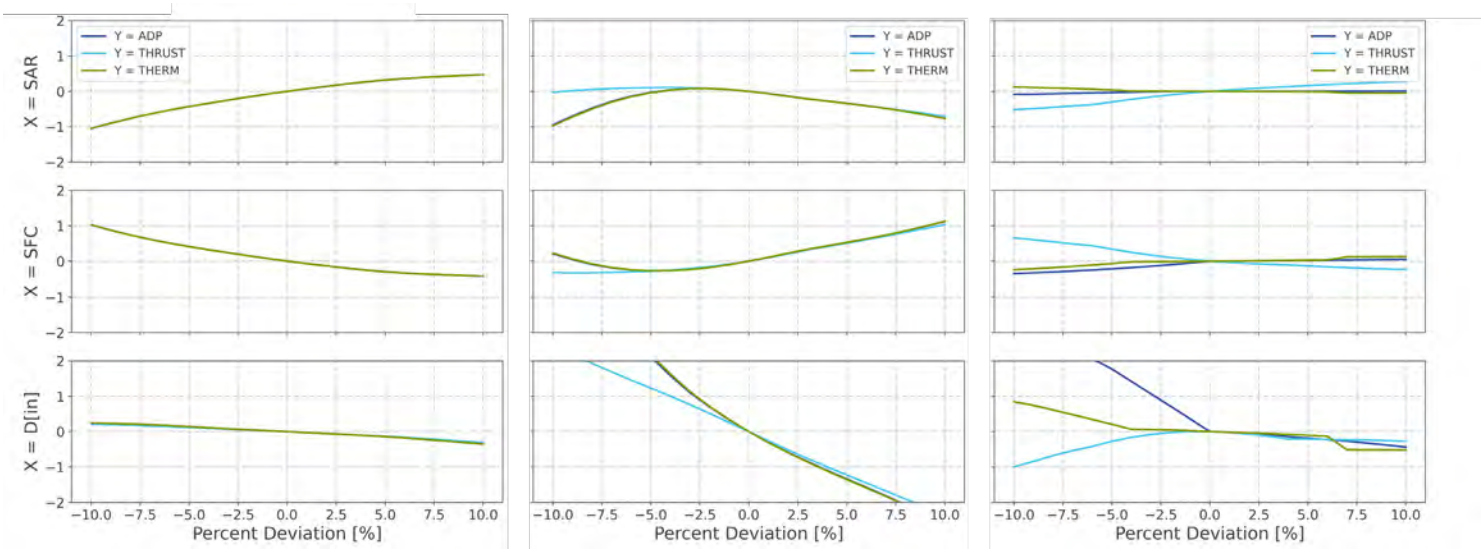

Figure 23. Sensitivity of metric *X* at the beginning of cruise to turbine inlet temperature (left), corrected fan speed (middle), and time (right) at point *Y*.

Mixed Versus Unmixed Performance

An analysis comparing the performance of mixed and unmixed engines performing the STCA mission was also performed, in which mixed engines performed better than unmixed equivalents with respect to fuel mass and efficiency. Specifically, we obtained a 2.2% increase in overall efficiency, broken into a 3.7% gain in thermal, or inner, efficiency and a 1.0% loss in propulsive efficiency. The flow mixer allows some of the hot core stream's thermal energy to be usefully converted to kinetic energy in the cool bypass stream. This energy would otherwise be effectively wasted, as isentropic expansion cannot usefully bring the exhaust to ambient temperature. The effect of this is two-fold. First, the increase in kinetic energy across the mixer increases mass-averaged velocity of the exhaust, decreasing propulsive efficiency by a small amount. Second, the kinetic energy increase effectively reduces requirements on the upstream components. This allows for a decrease in bypass stream size from a fan pressure ratio of 2.17 to 1.80 and from a fan diameter of 1.40 m to 1.26 m. The decreased fan power requirement results in less power dissipating in the turbine and mechanical transfer, boosting the thermal efficiency.

The increase in overall efficiency is balanced by the added mass of a lobed mixer. On a lower fan diameter engine such as an SST aircraft, the mixer mass is relatively low. A similar analysis performed on ultra-high bypass subsonic engines yielded a mixer mass just over twice that for SST, leading to a decrease in useful payload. As such, we conclude that lobed flow mixer should only be considered for low fan diameter applications.

Publications

None.

Outreach Efforts

None.

Awards

None.

Student Involvement

This work was performed primarily by graduate research assistant Wyatt Giroux, working under the supervision of Dr. Prakash Prashanth, Dr. Jayant Sabnis, Dr. Raymond Speth, and Dr. Choon Tan.

References

Berton, J. J., Huff, D. L., Geiselhart, K., & Seidel, J. (2020, January 6-10). *Supersonic technology concept aeroplanes for environmental studies* [Conference presentation. AIAA Scitech 2020 Forum, Orlando, Florida. https://doi.org/10.2514/6.2020-0263

Claus, R. W., Evans, A. L., Lylte, J. K., & Nichols, L. D. (1991). Numerical propulsion system simulation. *Computing Systems in Engineering*, *2*(4), 357–364. https://doi.org/10.1016/0956-0521(91)90003-N

Kang, S., Roumeliotis, I., Zhang, J., Broca, O., & Pachidis, V. (2022). Assessment of engine operability and overall performance for parallel hybrid electric propulsion systems for a single-aisle aircraft. *Journal of Engineering for Gas Turbines and Power*, *144*(041002). https://doi.org/10.1115/1.4052880

Lammen, W., & Vankan, J. (2020, January 6-10). *Energy optimization of single aisle aircraft with hybrid electric propulsion* [Conference presentation]. AIAA Scitech 2020 Forum, Orlando, Florida. https://doi.org/10.2514/6.2020-0505

Lents, C. E., Hardin, L. W., Rheaume, J., & Kohlman, L. (2016, July 25-27). *Parallel hybrid gas-electric geared turbofan engine conceptual design and benefits analysis* [Conference presentation]. 52nd AIAA/SAE/ASEE Joint Propulsion Conference, Salt Lake City, Utah. https://doi.org/10.2514/6.2016-4610

Prashanth, P., Voet, L. J. A., Speth, R. L., Sabnis, J. S., Tan, C. S., & Barrett, S. R. H. (2023). Impact of design constraints on noise and emissions of derivative supersonic engines. *Journal of Propulsion and Power*, *39*(3), 1–10. https://doi.org/10.2514/1.B38918

Seddon, J., & Goldsmith, E. L. (1999). *Intake aerodynamics*. American Institute of Aeronautics and Astronautics Education Series.

Seitz, A., Nickl, M., Stroh, A., & Vratny, P. C. (2018). Conceptual study of a mechanically integrated parallel hybrid electric turbofan. *Proceedings of the Institution of Mechanical Engineers, Part G: Journal of Aerospace Engineering*, *232*(14), 2688–2712. https://doi.org/10.1177/0954410018790141

Task 6 - Assess the Effect of Variable Noise Reduction Systems on LTO Emissions for Engines for Supersonic Transport Aircraft

Massachusetts Institute of Technology

Objective

The engine configurations currently being pursued for the second-generation SST are low or medium bypass turbofans, instead of afterburning turbojets used on Concorde. Such engines, sized for supersonic cruise, are likely to have higher thrust capability at the take-off condition and therefore, may be able to use a programmed thrust cutback (PTCB), allowing the aircraft to perform a take-off at less than 100% of the thermodynamically available thrust. Unlike thrust lapse, PTCB is not a thermodynamic, aerodynamic, nor atmospheric phenomenon but rather, it is a computer-programmed reduction in thrust during the take-off procedure of the aircraft for the purpose of reducing certification noise.

A PTCB designed to reduce certification noise has an impact on the amount of gaseous emissions from the engines during take-off procedures (in this work only NO_x emissions are considered). The objective of this task is to analyze whether a single thrust-setting for the climb-out phase of the engine emissions LTO cycle is representative, or whether the PTCB should be accounted for in the engine emissions LTO cycle.

The objective of this task involves interdependencies between aircraft operations related to PTCB and engine emission certification standards. The noise certification flight profile is chosen as a reference flight profile to analyze these interdependencies. The in-flight emissions during the climb-phase (between 35 ft and 3000 ft) of the noise reference trajectories resulting from different PTCB trajectories are compared to the emissions of the climb mode of the engine emission LTO certification standard. The comparison is done both for the existing subsonic and supersonic engine emission LTO certification standard to assess which is more representative.

Research Approach

The approach employed to address the above-mentioned research objectives is shown in Figure 22. We start from a supersonic aircraft model and an engine model for that aircraft. These are input in a take-off trajectory model that is coupled to a noise model. Minimizing the noise footprint using a variable noise reduction system, gives us a PTCB, characterized by a thrust-setting schedule as a function of time, $\mathrm{TS}(t)$. This thrust-setting schedule is put into a combustor model to estimate take-off emissions (i.e., Method 1 in Figure 22). These emissions are then compared to those in a

baseline trajectory, using a simple power setting schedule, without variable noise reduction systems (VNRS) being applied (i.e., Method 2 in Figure 22). We are interested in comparing the take-off emissions of both these methods.

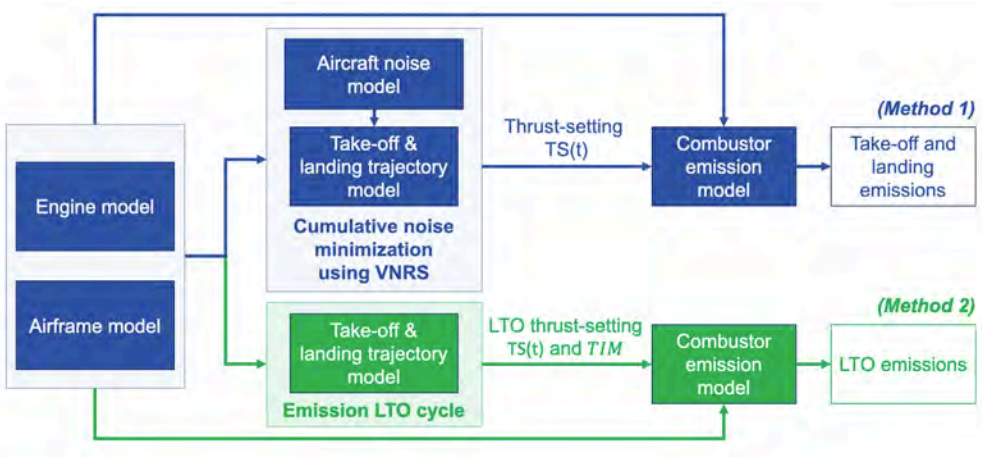

Figure 24. Flow chart of the approach to estimate the effect of VNRS on take-off emissions of engines for SST.

LTO Engine Emissions Certification Cycles

The current subsonic and supersonic LTO emissions cycles indicating thrust setting and time in mode for the different phases are shown in Table 8 and Table 9, respectively (ICAO, 2017b).

Table 8. Subsonic LTO engine emissions certification cycle.

Subsonic Operating Mode	Subsonic Engine Power (percentage of standard day sea-level static thrust, F_{00})	Subsonic Time in Mode
Idle (taxi)	7%	26.0 min
Take-off	100%	0.7 min
Climb out	85%	2.2 min
Approach	30%	4.0 min

Table 9. Supersonic LTO engine emission certification cycle.

Supersonic Operating Mode	Supersonic Engine Power (percentage of standard day sea-level static thrust, F_{00})	Supersonic Time in Mode
Idle (taxi)	5.8%	26.0 min
Take-off	100%	1.2 min
Climb out	65%	2.0 min
Descent	15%	1.2 min
Approach	34%	2.3 min

Modelling Take-off Trajectories

The reference take-off trajectory is composed of five phases, summarized in Table 10. During the ground roll phase, the aircraft accelerates until it reaches rotation speed, $V_{\mathrm{rot}} = k_{\mathrm{rot}} V_{\mathrm{stall}}$ (with k_{rot}=1.3). In the rotation phase, the aircraft pitches up, increasing its angle of attack, α, with a constant rate ($d\alpha/dt$ = 3.5 deg/s) until its net upward force is zero. In the climb phase, the aircraft climbs until it reaches the obstacle height, z_{obstacle}, after which the programmed thrust cutback, $\mathrm{TS}_{\mathrm{PTCB}}$, and pilot-initiated cutback, $\mathrm{TS}_{\mathrm{cb}}$, is applied is applied in the PTCB and cutback phases, respectively. The trajectory stops when the aircraft reaches an altitude $z_{\mathrm{end}} = 1500\ \mathrm{m}$. The first three phases of the take-off trajectory are performed using a

take-off thrust setting $\mathrm{TS_{TO}} = 100\%$. The angle-of-attack, α, serves as control parameter in the climb PTCB and cutback phase and its schedule is determined by optimizing the trajectory for the minimum time to climb to $z_{\mathrm{end}} = 1500\ \mathrm{m}$.

Table 10. Definition of take-off trajectory model.

Phase	Boundary constraint	Path constraint	Control parameters	
			α	TS
Ground roll	$V_{\mathrm{start}} = 0\ \mathrm{m/s} \rightarrow v_{\mathrm{end}} = v_{\mathrm{rot}}$		$\alpha = \alpha_0$	TS=100%
Rotation	$\alpha_{\mathrm{start}} = \alpha_0 \rightarrow \alpha_{\mathrm{end}}\ \mathrm{s.t.}\ F_{\mathrm{up,end}} = 0$		$\frac{d\alpha}{dt} = \mathrm{const}$	TS=100%
Climb	$z_{\mathrm{start}} = 0 \rightarrow z_{\mathrm{end}} = z_{\mathrm{obstacle}}$	$\gamma > 4\%$* $v_{\mathrm{eas}} < 250\ \mathrm{kts}$	$\alpha = \alpha(t)$	TS=100%
PTCB	$z_{\mathrm{start}} = z_{\mathrm{obstacle}} \rightarrow z_{\mathrm{end}} = z_{\mathrm{cb}}$	$\gamma > 4\%$* $v_{\mathrm{eas}} < 250\ \mathrm{kts}$	$\alpha = \alpha(t)$	TS=$\mathrm{TS_{ptcb}}$
Cutback	$z_{\mathrm{start}} = z_{\mathrm{cb}} \rightarrow z_{\mathrm{end}} = 1500\ \mathrm{m}$	$\gamma > 4\%$* $v_{\mathrm{eas}} < 250\ \mathrm{kts}$	$\alpha = \alpha(t)$	TS=$\mathrm{TS_{cb}}$

* This path constraint can be replaced by the one-engine inoperative (OEI) condition.
α = angle of attack
TS = thrust setting

The allowable level of PTCB for the reference trajectory is governed by noise certification regulations and airworthiness standards (ICAO, 2017a): the thrust shall not be reduced below that required to maintain a minimum climb gradient of 4% or steady level flight with one engine inoperative (for multi-engine airplanes), whichever thrust is greater. The aircraft shall not have an indicated air speed of more than 250 kts at altitudes below 10,000 feet MSL. These limits are applied as path constraints of the reference take-off trajectory in Table 10.

Aircraft and Engine Modelling
In this task, two supersonic vehicles are analyzed that span 8–55 passengers and low supersonic (Mach 1.4) to high supersonic (Mach 2.2). The NASA STCA (Berton et al., 2020) is an 8-passenger supersonic business jet with cruise Mach number 1.4 (will be referred to as the NASA STCA). A larger 55-passenger supersonic airliner with cruise Mach number 2.2 designed by Georgia Institute of Technology (subsequently referred to as the M2.2 medium SST) is also analyzed. The engine used in the analysis of the effects of PTCB for the STCA aircraft is a derivative engine, based on the CFM56-5B core, while the engine used for the M2.2 medium SST is a clean-sheet engine (Voet et al., 2021).

Estimating NO_x Emissions
The P_3-T_3 method (DuBois & Paynter, 2006) is used to estimate the engine NO_x emissions. The P_3-T_3 method uses a polynomial regression to model the NO_x emissions from the combustor as a function of the combustor inlet pressure, P_{t3}, and temperature, T_{t3}. We use publicly available data on the NO_x emissions of the CFM56 family of engines from the ICAO EEDB (EASA, 2019) to determine the coefficients needed in our P_3-T_3 method. It is assumed that the emissions index of NO_x scales with $P_{t3}^{0.4}$ as shown in the following equation:

$$\frac{EI(NO_x)}{P_{t3}^{0.4}} = 6.26 \cdot 10^{-8} T_{t3}^3 - 1.17 \cdot 10^{-4} T_{t3}^2 + 0.074 T_{t3} - 15.04 \qquad \text{(Eq. 2)}$$

Since the production of NO_x in a RQL combustor is primarily controlled by the flame temperature and the mixing of the primary zone gas, it is assumed that the above P_3-T_3 correlation is representative of the emissions we expect from a derivative engine that uses the CFM56 core.

The clean-sheet engine designed for the M2.2 medium SST is also assumed to have the same combustor technology as in the STCA engine as well as the CFM56-5B3. This allows us to use the same P_3-T_3 model to estimate emissions of NO_x from the combustor and facilitates a comparison between the two aircraft-engine pairs while holding the combustor technology fixed.

Modeling Take-off Noise
The take-off certification noise levels - in terms of the lateral and flyover effective perceived noise level - are computed using the aircraft noise estimation model, developed as part of Task 3. The side-line (lateral) and flyover noise metrics, defined by ICAO Annex 16 (ICAO, 2017a) are computed for each of the take-off trajectories in the design space. The flyover microphone is located at 6500 m downstream of break release; the location of the lateral microphone is located 450 m away from the runway center line at the position of maximum sideline noise.

Milestone

- Estimated the differences of NO_x pollutant emissions of engines for SST aircraft flying a range of trajectories varying VNRS for two different aircraft configurations.

Major Accomplishments

Estimate of PTCB Range Based on Trajectory Simulations
The possible range of PTCB for the two supersonic vehicles is estimated using take-off trajectory simulations. A single pilot-initiated cutback maneuver is analyzed for the STCA and M2.2 medium SST. The cutback procedure is described by two parameters, namely a cutback altitude, z_{cb}, and a cutback thrust setting, TS_{cb}. The design-space of the single-cutback PTCB is explored by varying both parameters: $z_{cb} \in [25, 750]\text{m}$ and $TS_{cb} \in [50, 100]\%$ for the STCA and $TS_{cb} \in [60, 100]\%$ for the M2.2 medium SST. Thrust settings outside these ranges fail to meet the noise certification and airworthiness requirements for the respective vehicles. A take-off thrust setting $TS_{TO} = 100\%$ is employed. Sample trajectories with and without cutback are shown for the STCA and M2.2 medium SST in Figure 23.

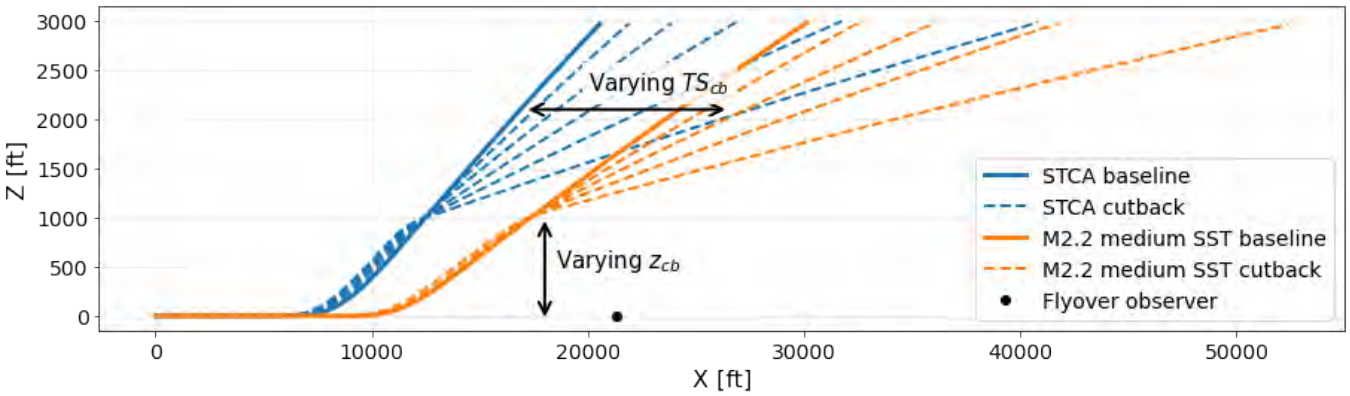

Figure 25. Example of single thrust cutback trajectories for STCA and M2.2 medium SST for $\boldsymbol{z_{cb}}$=1000ft and $\boldsymbol{TS_{cb}} \in [\mathbf{50}, \mathbf{100}]\%$ (for STCA) and $\boldsymbol{TS_{cb}} \in [\mathbf{60}, \mathbf{100}]\%$ (for M2.2 medium SST). The baseline trajectory has a constant thrust setting TS=100%.

The lateral, flyover and cumulative effective perceived noise level as a function of TS_{cb} and z_{cb} is plotted for the single thrust cutback of the STCA and M2.2 medium SST in Figure 24 and Figure 25, respectively.

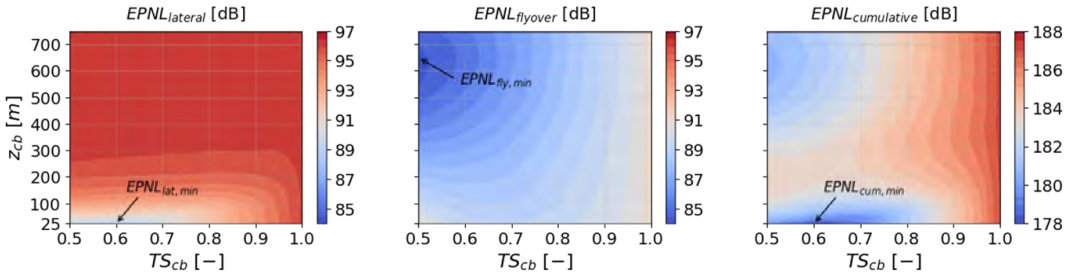

Figure 26. Lateral, flyover and cumulative noise reduction for single cutback trajectories of the STCA.

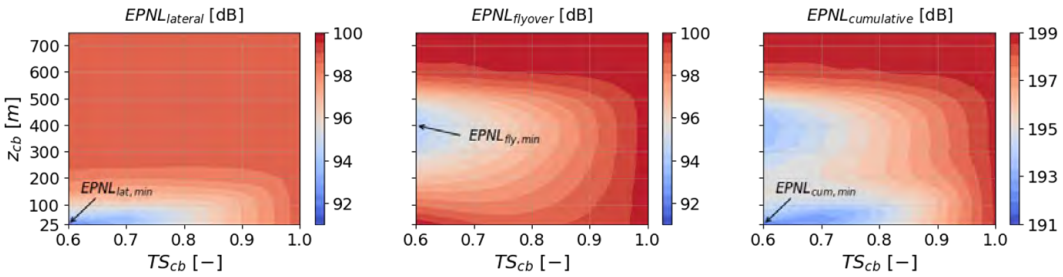

Figure 27. Lateral, flyover and cumulative noise reduction for single cutback trajectories of the M2.2 medium SST.

In Figure 24 and Figure 25, a cutback at low altitudes monotonically decreases the lateral EPNL for both vehicles. A cutback at altitudes z_{cb} > 200 m does not result in improvement in lateral noise anymore, as the aircraft is already past the region of influence of the lateral microphone. For the flyover microphone, a local minimum exists at z_{cb}=650 m for the STCA and at z_{cb}=400 m for the M2.2 medium SST; cutting back later results in more source noise at the flyover microphone and cutting back earlier results in a smaller distance between the aircraft and the flyover microphone increasing noise. For both vehicles, the lateral noise reduction dominates the cumulative noise reduction. Therefore, the point in the feasible design space that results in the minimum cumulative noise occurs at ($TS_{cb} = 60\%, z_{cb} = 25$ m) for both vehicles.

The single cutback minimum noise trajectory is considered a lower bound on the thrust setting during climb-out, whereas a trajectory without any cutback is considered an upper bound. Two additional trajectories, i.e., a standard and advanced trajectory based on the NASA STCA noise assessment (Berton et al., 2020), are also considered with thrust cutbacks in between these bounds. The definitions of these four reference trajectories are shown in Table 11 and their thrust-setting schedules are illustrated in Figure 26.

Table 11. Comparison of reference trajectories.

Name	TS_{TO}	PTCB		Pilot-initiated cutback	
		h_{cb}	TS_{cb}	h_{cb}	TS_{cb}
No cutback	100%	-	-	-	-
Standard	100%	-	-	584.7m	65%
Advanced	100%	15.3m	85%	544.1m	65%
Single CB min. noise	100%	25m (M 1.4, 8 pax) 25m (M2.2, 55pax)	60% (M 1.4, 8 pax) 65% (M 2.2, 55 pax)	-	-

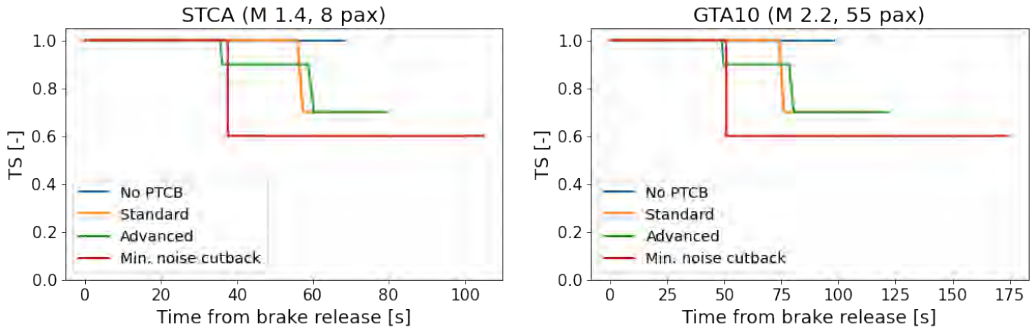

Figure 28. Thrust-setting schedules for trajectories in Table 11 for the STCA and M2.2 medium SST.

Instantaneous Engine Conditions at Various PTCB Levels During Climb Out

The thermodynamic conditions at the inlet to the combustor, T_{t3} and P_{t3}, are shown by the shaded region in Figure 27 at various climb thrust settings for the STCA. The flight Mach number is varied from 0.2 to 0.48 (typical Mach numbers between the aircraft stall speed and $v_{eas} = 250$ kts) and the flight altitude from 500 to 3000 ft (LTO is considered to consist only of flight phases below 3000 ft altitude). The thermodynamic conditions are normalized by the ICAO LTO conditions for a climb out thrust setting, i.e., 85% of the sea-level static thrust, F_{00}. The thermodynamic conditions for the three cutback trajectories are shown in Figure 27.

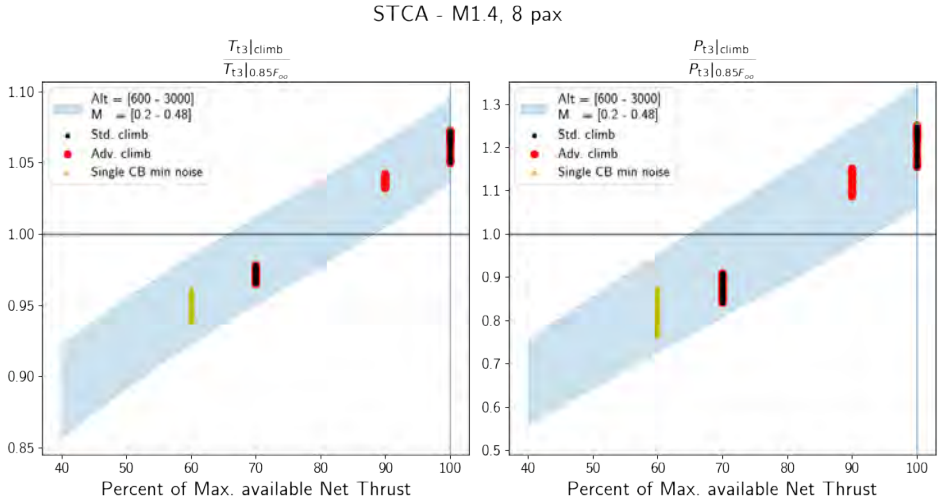

Figure 29. Combustor inlet conditions (P_{t3}, T_{t3}) for flight Mach numbers M ∈ [0.2, 0.48] and altitudes Alt ∈ [500, 3000] ft for the NASA STCA. The black marker and horizontal line indicate the sea-level static conditions at the corresponding thrust setting (TS). The sea level static (SLS) value at 85% F_{oo} corresponds to the ICAO LTO climb out thrust level.

Figure 27 shows that, for the possible range of PTCB identified, the temperature at the inlet to the combustor for the STCA can vary between ~7% below to ~8% above that at the ICAO LTO climb out thrust setting. The pressure at the combustor inlet can vary between ~30% below to 25% above that of ICAO LTO climb out thrust setting.

The instantaneous emission index of nitrogen oxides (EI(NO_x)) for the four trajectories listed in Table 11 are shown in Figure 28. The take-off and climb-out phase of the subsonic certification and supersonic certification LTO cycle are also indicated for reference.

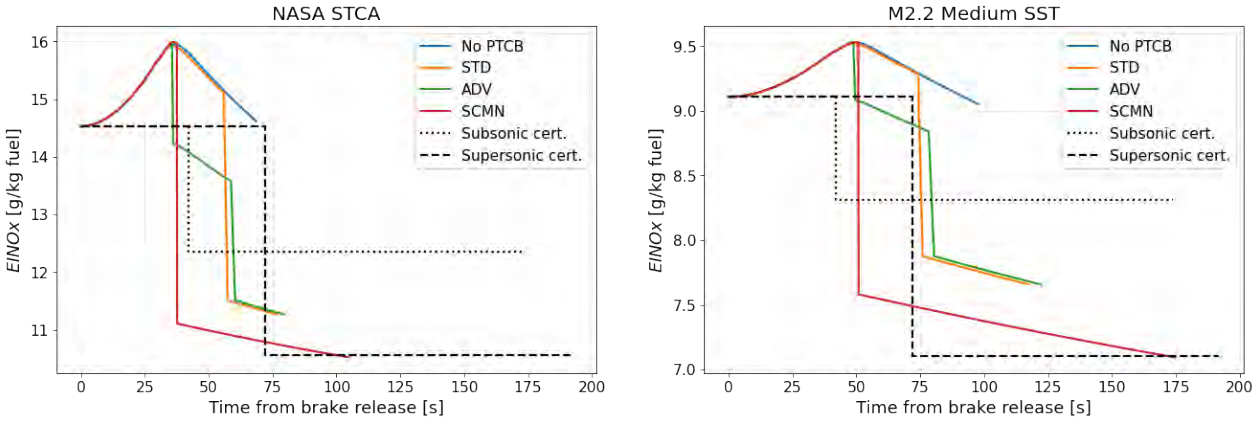

Figure 30. Trajectory instantaneous EI(NO_x) compared to the subsonic and supersonic certification.

The EI(NO_x), during the climb phase relative to the emission index (EI) at the 85% F_{oo} LTO value is shown in Figure 29. We show the trends of the EI(NO_x) values for various PTCB cutback levels for the STCA and M2.2 medium SST.

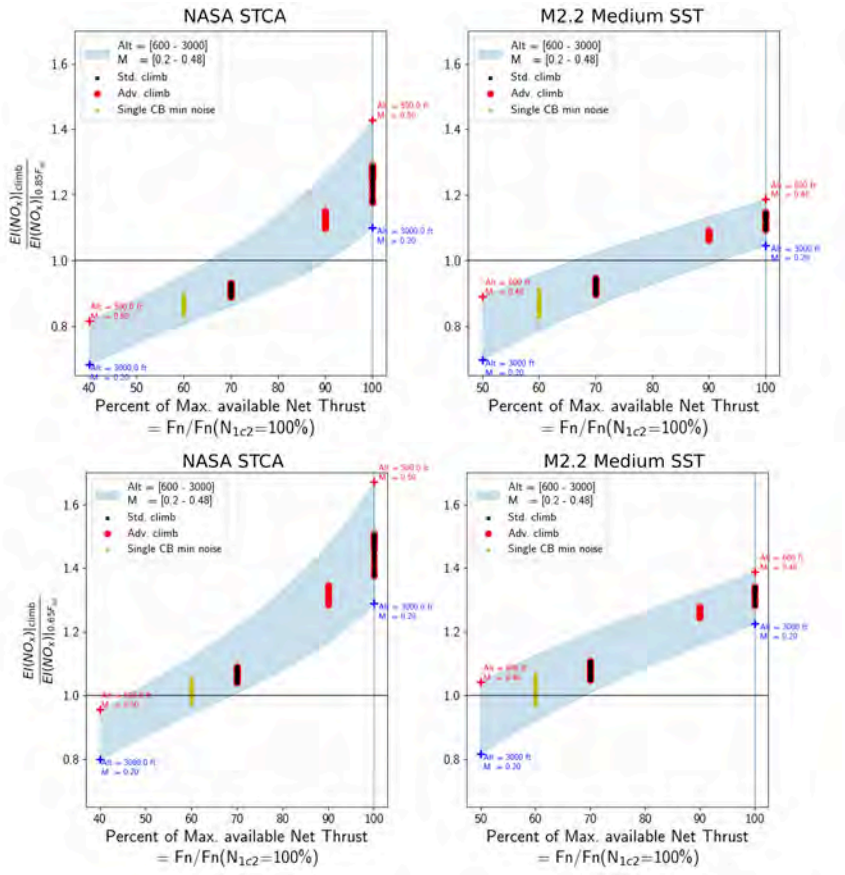

Figure 31. NO_x emissions relative to the 85% (top row) and 65% (bottom row) LTO thrust setting for various flight conditions for two example SST – the 8 passenger M1.4 NASA STCA and M2.2 Medium SST. The black markers indicate the sea-level static conditions at the corresponding thrust setting.

The overall compressor pressure rise (inlet of fan root to combustor inlet) is limited by the maximum allowable T_{t3} based on the materials used in the engine. As the cruise Mach number increases, i.e., from M=1.4 for the STCA to M=2.2 for the M2.2 medium SST) the ram compression increases the inlet temperature and therefore, the allowable compressor pressure ratio reduces. The lower design pressure ratio for the M2.2 medium SST implies a lower T_{t3} in the LTO cycle relative to the STCA. Therefore, the combustor inlet temperatures (and consequently NO_x emissions) are driven by the compressor pressure ratio.

Figure 29 shows that the trend of EI(NO_x) varies for the different aircraft. The STCA climb profile shows that at a 65% thrust setting the EI(NO_x) is approximately 7-12% lower than the LTO value. However, at a thrust setting of 50% (determined by the minimum noise trajectory for a single full-authority digital engine control [FADEC]-controlled cutback event) the EI(NO_x) is 12-20% lower than the LTO value. If the available thrust during climb is higher than the required thrust the PTCB level can be higher (leading to lower TS) and therefore, even lower EI(NO_x) relative to the LTO 85% value. On the other hand, if the required thrust is close to the available thrust then the PTCB level will be lower resulting in EI(NO_x) values greater than the 85% LTO value. For the M2.2 medium SST, at a 65% thrust setting we observer an EI(NO_x) that is ~10% lower than the LTO value. These variations are in part due to the lower required compressor pressure ratios as the cruise Mach number increases. This indicates that the deviation from the LTO 85% value is dependent on the aircraft-engine combination. The

variation in the trends of EI(NO_x) at various flight conditions is observed in the difference between the shaded regions for the two aircraft under consideration.

We observe that the spread of the normalized EI(NO_x) for the STCA is larger at 100% thrust setting relative to the 50% thrust setting. In contrast, the spread at the 100% thrust setting is smaller than the 50% thrust setting for the M2.2 aircraft. This is due to the sensitivity of EI(NO_x) predicted by the P_3-T_3 model to T_{t3}. At lower temperatures ~500-550 K the slope of the EI(NO_x) vs. T_{t3} is higher than the slope at temperatures of 600-650 K. Therefore, for similar variation in T_{t3} the variation in EI(NO_x) is larger for the M2.2 aircraft at lower thrust settings than the STCA.

Estimate of Difference in Integrated Emissions Between Reference Trajectories and LTO Certification Cycles During Climb-Out

The cumulative mass of NO_x emitted from 35 ft up to 3000 ft for the four trajectories is shown in Figure 30 and Figure 31 for the NASA STCA and M2.2 Medium SST, respectively. The comparison of the final cumulative mass of NO_x with the subsonic and supersonic certification LTO cycle, i.e., $m_{NO_x,35<h<3000ft}/m_{NO_x,cert.}$, is shown in Table 12. Note that, for the certification mass of NO_x emitted, $m_{NO_x,cert.}$, only the climb out phase is used.

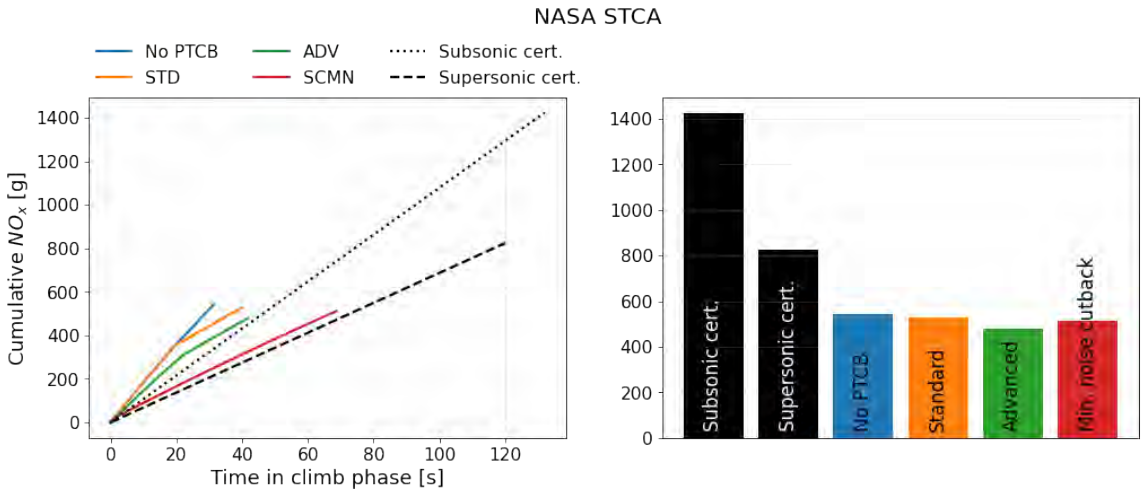

Figure 32. Integrated emissions comparison to subsonic and supersonic certification standards for the M1.4 STCA.

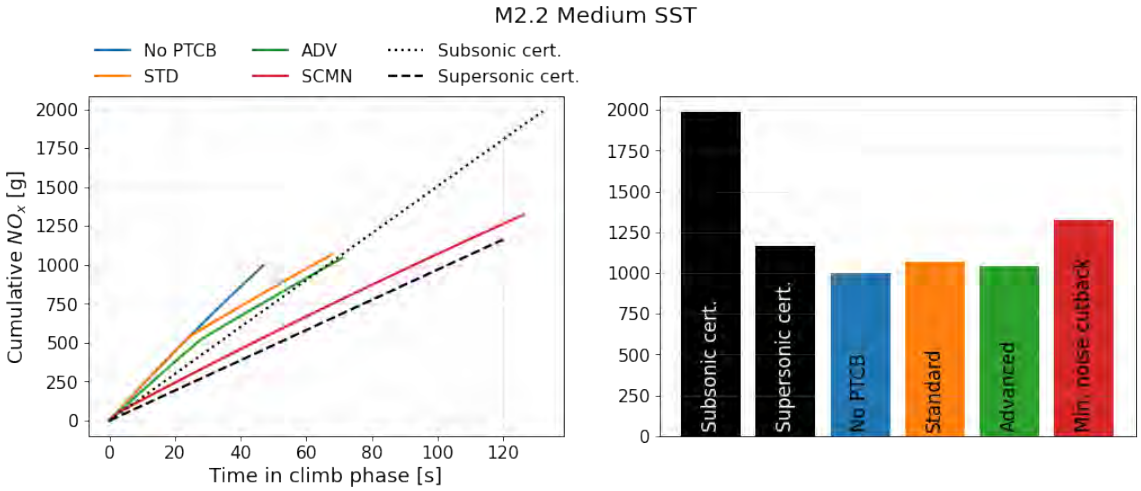

Figure 33. Integrated emissions comparison to subsonic and supersonic certification standards for the M2.2 medium SST.

A comparison of the integrated emissions has been made on a D_p/F_{oo} basis, where only the take-off and climb phases are considered (therefore, further referred to as m_{NO_x}/F_{oo}). The difference in m_{NO_x}/F_{oo} between the four trajectories and the subsonic and supersonic certification LTO cycle are shown in Table 12.

Table 12. Comparison of the climb out $\boldsymbol{m_{NO_x}/F_{oo}}$ ($35 < \boldsymbol{h} < 3000$ ft) for the STCA and M2.2 medium SST with subsonic and supersonic certification LTO cycles (+ means certification cycle is overestimating).

Trajectory name	NASA STCA			M2.2 medium SST		
	$\frac{m_{NO_x}}{F_{oo}}\left[\frac{g}{kN}\right]$	$\Delta_{subsonic}$ [%]	$\Delta_{supersonic}$ [%]	$\frac{m_{NO_x}}{F_{oo}}\left[\frac{g}{kN}\right]$	$\Delta_{subsonic}$ [%]	$\Delta_{supersonic}$ [%]
Subsonic certification	17.8	-	-	14.6	-	-
Supersonic certification	10.3	-	-	8.5	-	-
No cutback	6.8	+61.9	+34.2	7.3	+49.7	+14.1
Standard	6.6	+63.0	+36.1	7.8	+46.3	+8.3
Advanced	6.0	+66.3	+41.8	7.7	+47.4	+10.2
Single CB min. noise	6.4	+64.1	+37.9	9.7	+33.5	-13.6

Table 12 shows that for the STCA aircraft the subsonic certification climb-out time in mode and thrust setting overestimates the mass of NO_x emissions per unit thrust (m_{NO_x}/F_{oo}) of real trajectories by 64% (for the single cutback minimum noise trajectory) to 62% (for no cutback). The supersonic certification time in mode and thrust setting also overestimates m_{NO_x}/F_{oo}, but by smaller margins - 38% to 34% (for the single cutback minimum noise trajectory and no cutback trajectory respectively). For the M2.2 medium SST the subsonic certification climb-out time in mode and thrust setting overestimates m_{NO_x}/F_{oo} by 33.5% to 50%. While the supersonic certification climb-out time in mode and thrust-setting underestimates the m_{NO_x}/F_{oo}, of real single cutback minimum noise trajectory by -13.6% and overestimates m_{NO_x}/F_{oo}, for the no cutback trajectory by 14%, the margin is smaller than the subsonic rules. This suggests that the thrust setting prescribed by the current supersonic certification LTO climb out mode, i.e., 65% F_{oo} is more representative of the real trajectories of the M1.4 STCA and M2.2 Medium SST than the subsonic certification thrust setting of 85% F_{oo}.

Publications
None.

Outreach Efforts
- Mr. Laurens Voet presented an Information Paper titled "Investigation of the effects of VNRS on LTO emissions of engines for supersonic transport aircraft" at the CAEP/12-WG3/5-ESTG meeting on November 3, 2020.
- Mr. Laurens Voet gave a presentation titled "Development of optimal control framework to design VNRS for take-off operations of civil supersonic transport" at NASA Glenn Research Center on July 22, 2021.
- Mr. Laurens Voet gave a presentation titled "Design of variable noise reduction systems for civil supersonic transport certification noise reduction" at the NASA Acoustics Technical Working Group Meeting Fall 2021 on October 19, 2021.

Awards
None.

Student Involvement
This task was conducted primarily by graduate research assistant Laurens Voet, working under the supervision of Dr. Jayant Sabnis, Dr. Raymond Speth, and Dr. Choon Tan.

References
Berton, J. J., Huff, D. L., Geiselhart, K., & Seidel, J. (2020, January 6–10). *Supersonic technology concept aeroplane for environmental studies* [Conference presentation]. AIAA Scitech 2020 Forum, Orlando, Florida.

DuBois, D., & Paynter, G. C. (2006). Fuel Flow Method 2 for estimating aircraft emissions (SAE Technical Paper 2006-01-1987). SAE International.

EASA (2019). ICAO Aircraft Engine Emissions Databank, version 26A. European Union Aviation Safety Agency (EASA). https://www.easa.europa.eu/easa-and-you/environment/icao-aircraft-engine-emissions-databank

ICAO. (2017a). *Annex 16 to the Convention on International Civil Aviation: Environmental Protection - Volume 1: Aircraft Noise* (8th Ed). International Civil Aviation Organization (ICAO).

ICAO. (2017b). *Annex 16 to the Convention on International Civil Aviation: Environmental protection - Volume II: Aircraft engine emissions* (4th Ed). International Civil Aviation Organization (ICAO).

Voet, L., Prashanth, P., Speth, R., Sabnis, J., Tan, C., & Barrett, S. (2021, January 11–15 & 19–21). *The impact of design space constraints on the noise and emissions from derivative engines for civil supersonic aircraft* [Conference presentation]. AIAA Scitech 2021 Forum, virtual.

Task 7 - Evaluate the Impact of Advanced Take-off Trajectories for SST Using VNRS on Community Noise
Massachusetts Institute of Technology

Objectives
The objective of this task is to extend our evaluation of the noise impacts of advanced take-off trajectories to incorporate VNRS. These advanced take-off trajectories are designed and optimized by using the take-off certification noise level as a representative metric for noise around airports. The take-off certification noise level incorporates noise levels measured at two locations, i.e., the lateral and flyover microphones. To assess whether these advanced take-off trajectories are effective in community noise reduction, we calculate community noise contours.

Research Approach
Figure 32 summarizes the noise levels of the advanced take-off trajectories for the NASA STCA using VNRS as measured using the certification noise metric. Reduced cut-back altitudes (from 260 m to 11 m) and increased take-off speeds (from 200 kts to 250 kts) enable as much as 7 EPNdB of cumulative noise reduction. When continuous thrust control (also described as programmed thrust cutback) is used, an additional 3.6 EPNdB of cumulative noise reduction can be achieved. The inherent tradeoff between lateral and flyover noise for the discrete high-altitude and low-altitude thrust cut-back trajectories can be seen in Figure 32. At increased take-off speed, the advanced take-off trajectory with continuous thrust

control avoids this tradeoff by reducing flyover noise without increasing lateral noise, with respect to those with the low-altitude cutback.

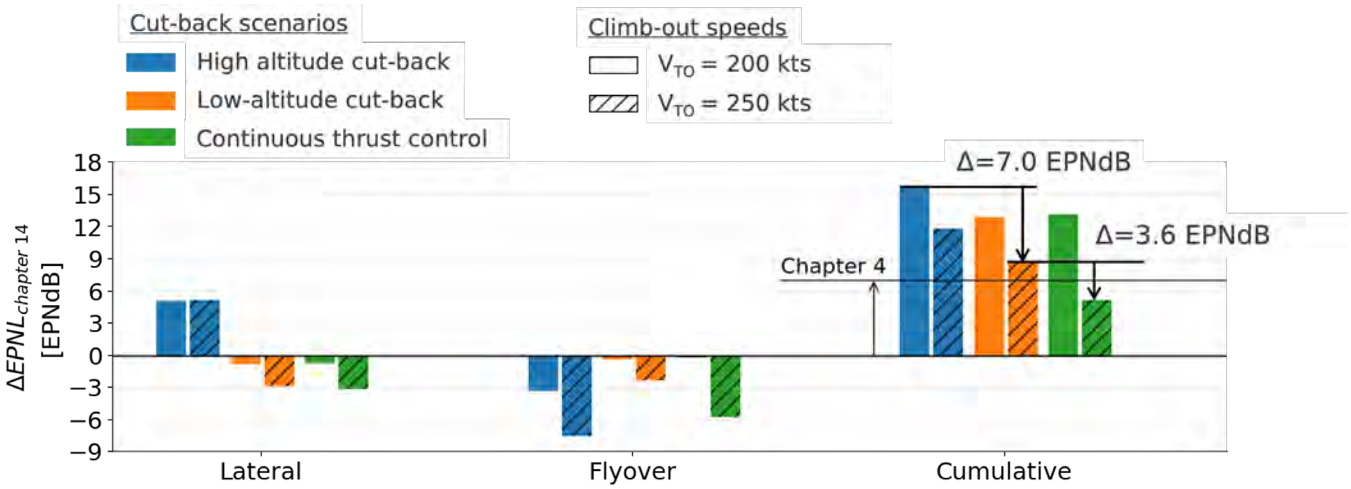

Figure 34. Comparison of the lateral, flyover, and cumulative certification noise levels of standard and advanced trajectories with the ICAO Annex 16 Chapter 14 noise limits (ICAO, 2017). The Annex 16 Chapter 4 noise limits are also indicated for reference.

Programmed high-lift devices have been found to be ineffective in reducing take-off noise for the NASA STCA. Figure 32 shows that, even with the use of advanced take-off trajectories, the NASA STCA is unable to meet current noise limits for subsonic transport set by the ICAO in Annex 16, Volume 1, Chapter 14 (ICAO, 2017). Additional noise reduction might be achieved by incorporating reduced thrust take-off procedures, as explored by Berton et al. (2019) and Olson (1992).

The impact of the advanced take-off trajectories on community noise is shown in the SEL line contours and ΔSEL color contours in Figure 33. In Figure 33, the top left plot shows the community noise contours for the standard take-off trajectory, abiding by the current noise standards for subsonic transport in ICAO Annex 16. The noise is highest underneath the flight path on the centerline and decreases when laterally moving away in the *y*-direction. The center plot on the top row shows the ΔSEL between the high-altitude and low-altitude cut-back.

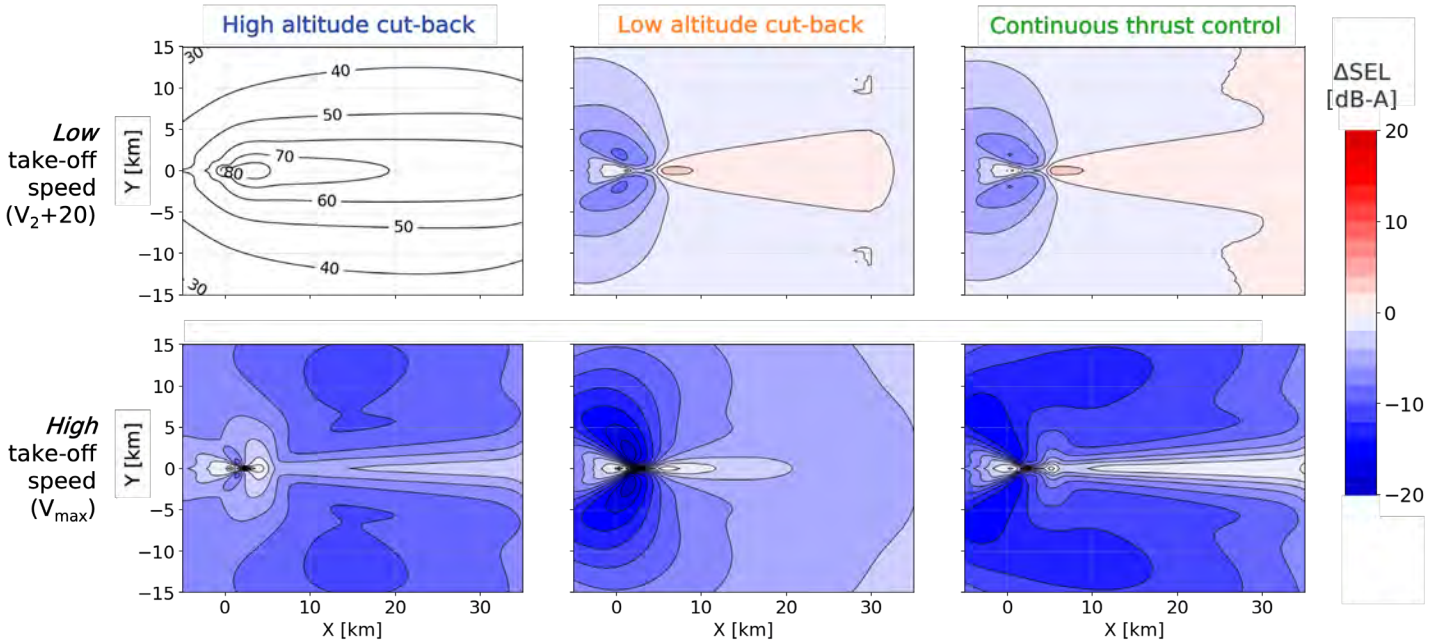

Figure 35. SEL line contours for the NASA STCA standard single thrust cut-back trajectory abiding by the noise standards for subsonic transport defined in ICAO Annex 16 (top left). ΔSEL color contours for the NASA STCA advanced take-off trajectories (top middle and top right, bottom row). The origin is the aircraft brake release point.

With the low-altitude cutback, the community noise contours show the tradeoff between points in the airport vicinity and downstream, indicated by the blue and red regions. This tradeoff is also captured when the certification noise metric is used. At increased take-off speeds, the same tradeoff is observed; however, the average noise is reduced because of the reduced jet shear at higher take-off speeds.

The high-altitude cutback achieves the largest noise reduction in downstream regions, whereas the low-altitude cut-back achieves the largest noise reduction in regions in the vicinity of the airport. With continuous thrust control (at increased take-off speeds), the advanced take-off trajectory achieves noise reduction in the combined region between airport vicinity and downstream. Overall, this trajectory achieves the largest noise reduction relative to all other advanced take-off trajectories.

Figure 34 compares the community noise contours for the high-speed advanced take-off trajectories with continuous thrust control and low-altitude cut-back, i.e., the two trajectories with lowest cumulative noise levels when the certification noise metric is used. With the continuous thrust control trajectory, noise is reduced in the areas where it was already low (away from the flight path, as shown in the line contour of Figure 34), and is not reduced underneath the flight path, where the noise was the highest. These findings illustrate where the certification and community noise metrics are not aligned and thus suggest re-examination of the certification noise metric for SST using advanced take-off trajectories.

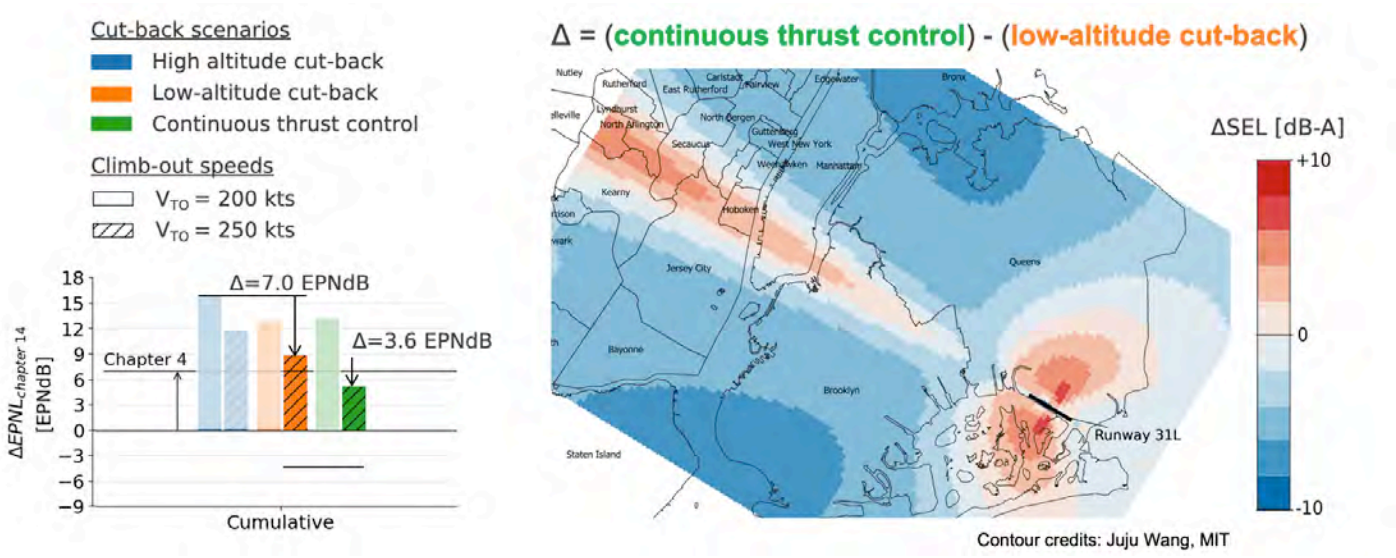

Figure 36. Comparison of certification cumulative noise levels between high-speed continuous thrust control and low-altitude cut-back trajectories (left). ΔSEL color contours for high-speed continuous thrust control and low-altitude cut-back trajectories taking off from runway 31L at New York JFK airport (right).

Milestones

- Used the pyNA aircraft noise estimation tool (Voet et al., 2021) to calculate the community noise contours around airports for the advanced take-off trajectories for SST using VNRS.
- Applied the community noise contours to an existing airport. In this work, the New York John F. Kennedy (JFK) airport is chosen. The departure from JFK is from Runway 31L.

Major Accomplishments

- Applied the use of continuous thrust control (also described as programmed thrust cutback) to achieve an additional 3.6 EPNdB of cumulative noise reduction. At increased take-off speed, the advanced take-off trajectory with continuous thrust control avoids this tradeoff by reducing flyover noise without increasing lateral noise, with respect to those with the low-altitude cutback.
- Found programmed high-lift devices to be ineffective in reducing take-off noise for the NASA STCA.
- Identified that certification and community noise metrics are not aligned, suggesting re-examination of the certification noise metric for SST using advanced take-off trajectories.

Publications

Voet, L., Speth, R. L., Sabnis, J. S., Tan, C. S., & Barrett, S. R. (2022, June 14). *On the design of variable noise reduction systems for supersonic transport take-off certification noise reduction* [Conference presentation]. 28th AIAA/CEAS Aeroacoustics 2022 Conference, Southampton, United Kingdom. https://doi.org/10.2514/6.2022-3052

Voet, L. J. A., Prashanth, P., Speth, R. L., Sabnis, J. S., Tan, C. S., & Barrett, S. R. H. (2024). Automatic Continuous Thrust Control for Supersonic Transport Takeoff Noise Reduction. *Journal of Aircraft*, *61*(1), 291–306. https://doi.org/10.2514/1.C037394

Outreach Efforts

- Presentation at the ASCENT Advisory Committee Spring Meeting (April 5–7, 2022)
- Presentation at the Aviation Emissions Characterization Roadmap Annual Meeting (May 24–26, 2022)

Awards

None.

Student Involvement

This task was conducted primarily by Laurens Voet, a graduate research assistant working under the supervision of Dr. Jayant Sabnis, Dr. Raymond Speth, and Dr. Choon Tan.

References

ICAO. (2017). *Annex 16 to the Convention on International Civil Aviation Environmental Protection Volume 1: aircraft noise* (8th Ed). International Civil Aviation Organization (ICAO).

Olson, E. D. (1992, September 30). *Advanced takeoff procedures for high-speed civil transport community noise reduction*. SAE International. https://doi.org/10.4271/921939

Voet, L., Prashanth, P., Speth, R., Sabnis, J., Tan, C., & Barrett, S. (2021). *The impact of design space constraints on the noise and emissions from derivative engines for civil supersonic aircraft*. [Conference Presentation] AIAA Scitech 2021 Forum. American Institute of Aeronautics and Astronautics. https://doi.org/10.2514/6.2021-1272